

Virtual Uniform Arrays: Enhancing the Degrees of Freedom for Direction-of-Arrival Estimation

by

Mien Khai GIANG

Submitted to the Department of Mathematical and Electrical Engineering

THESIS

at the

IMT ATLANTIQUE BRETAGNE-PAYS DE LA LOIRE

September 2025

© 2025 Mien Khai GIANG. All rights reserved.

Authored by: Mien Khai GIANG
 Department of Telecommunication Engineering
 August 27, 2025

Supervised by: Sébastien HOUCKE¹, Ahmed MASMOUDI¹, Thierry LE GALL²
 ¹Lecturer-Researcher, ²R&D Engineer

Virtual Uniform Arrays: Enhancing the Degrees of Freedom for Direction-of-Arrival Estimation

by

Mien Khai GIANG

Submitted to the Department of Mathematical and Electrical Engineering

THESIS

ABSTRACT

Most conventional Direction-of-Arrival (DoA) estimation techniques employing uniform arrays require that the number of receiving elements exceed the number of signal sources. This condition ensures an overdetermined system or the existence of a non-degenerate noise subspace, which is essential for covariance-matrix-based estimation algorithms. In this work, we propose a method to enhance the Degrees of Freedom (DoF) of a given set of physical antennas by modifying their relative positions to form an arbitrary two-dimensional planar array, thereby enabling the estimation of more sources than the number of physical sensors. The approach constructs the covariance matrix of a large virtual array from a smaller set of physical elements, allowing the application of classical subspace-based spectral estimation methods without being limited by the physical array size.

RÉSUMÉ

La plupart des techniques classiques d'estimation de la direction d'arrivée (DoA) utilisant des réseaux uniformes exigent que le nombre d'éléments de réception soit supérieur au nombre de sources. Cette condition garantit l'existence d'un système surdéterminé, ou d'un sous-espace de bruit non dégénéré, indispensable aux algorithmes d'estimation fondés sur la matrice de covariance. Dans ce travail, nous proposons une méthode visant à accroître les degrés de liberté (DoF) d'un ensemble donné d'antennes physiques en modifiant leurs positions relatives afin de former un réseau planaire bidimensionnel arbitraire. Cette approche permet d'estimer un nombre de sources supérieur à celui des capteurs physiques disponibles. Le principe consiste à construire la matrice de covariance d'un grand réseau virtuel à partir d'un plus petit ensemble d'éléments physiques, rendant possible l'application des méthodes classiques d'estimation spectrale basées sur les sous-espaces, sans être limitées par la taille du réseau physique.

Supervisors: Sébastien HOUCKE¹, Ahmed MASMOUDI¹, Thierry LE GALL²
Title: ¹Lecturer-Researcher, ²R&D Engineer

Acknowledgments

First of all, I would like to express my heartfelt thanks to Ho Chi Minh City University of Technology and IMT Atlantique Bretagne-Pays de la Loire for giving me the opportunity and favorable conditions to carry out this internship. I am also deeply grateful to the STICC laboratory for providing the equipment, technical support, and a welcoming environment that made the experimental work possible.

This thesis would not have been possible without the guidance, encouragement, and continuous support of Sébastien HOUCKE, Ahmed MASMOUDI, Thierry LE GALL, my colleagues and friends. I am especially thankful to Sébastien for his inspiring guidance, for proposing ideas and directions to develop the project, and for his brilliant suggestions whenever challenges arose, which encouraged me to explore the topic more creatively and strategically. I am truly grateful to Ahmed for his patience in carefully reviewing my reports multiple times, offering constructive feedback, and guiding me step by step to refine and improve this work; his advice on shaping the project and his support during experiments were invaluable. I would also like to sincerely thank Thierry for his generous and practical help with the hardware setup, for instructing me on necessary hardware usage, and for solving technical issues throughout the experimental process, as without his assistance the experiments could not have been successfully completed.

I would like to express my sincere gratitude to Huu Nhat HUYNH for inspiring the extended directions of this work, for his dedicated support throughout the experiments, and for his continuous encouragement that greatly helped me complete this thesis. Furthermore, I am deeply thankful for his patience, availability, and valuable discussions, which not only guided me in overcoming challenges but also motivated me to explore deeper insights into the subject. His enthusiasm has been a true source of inspiration throughout the process.

Lastly, I am deeply grateful for the unwavering support of my family, colleagues, and close friends, whose encouragement, trust, and belief in my work gave me the strength and determination to complete this journey.

Remerciements

Tout d'abord, je tiens à exprimer mes sincères remerciements à l'Institut polytechnique de Hô Chi Minh-Ville et à l'IMT Atlantique Bretagne-Pays de la Loire pour m'avoir offert l'opportunité et les conditions favorables afin de réaliser ce stage. Je suis également profondément reconnaissant envers le laboratoire STICC pour avoir fourni l'équipement, le soutien technique et un environnement accueillant qui ont rendu possible le travail expérimental.

Cette thèse n'aurait pas été possible sans les conseils, les encouragements et le soutien continu de Sébastien HOUCKE, Ahmed MASMOUDI, Thierry LE GALL, ainsi que de mes collègues et amis. Je suis particulièrement reconnaissant envers Sébastien pour ses orientations inspirantes, pour avoir proposé des idées et des directions afin de développer le projet, et pour ses suggestions brillantes chaque fois que des défis surgissaient, ce qui m'a encouragé à explorer le sujet de manière plus créative et stratégique. Je suis véritablement reconnaissant envers Ahmed pour sa patience à relire attentivement mes rapports à plusieurs reprises, à fournir des retours constructifs, et à me guider étape par étape pour affiner et améliorer ce travail ; ses conseils sur la structuration du projet et son soutien lors des expériences ont été inestimables. Je tiens également à remercier sincèrement Thierry pour son aide généreuse et pratique lors de la configuration du matériel, pour m'avoir instruit sur l'utilisation nécessaire du matériel, et pour avoir résolu les problèmes techniques tout au long du processus expérimental, car sans son assistance, les expériences n'auraient pas pu être menées à bien.

Je tiens à exprimer ma sincère gratitude à Huu Nhat HUYNH pour avoir inspiré les directions élargies de ce travail, pour son soutien dédié tout au long des expériences, et pour ses encouragements continus qui m'ont grandement aidé àachever cette thèse. De plus, je suis profondément reconnaissant pour sa patience, sa disponibilité et ses discussions précieuses, qui non seulement m'ont guidé pour surmonter les défis, mais m'ont également motivé à explorer des perspectives plus approfondies sur le sujet. Son enthousiasme a été une véritable source d'inspiration tout au long du processus.

Enfin, je suis profondément reconnaissant pour le soutien indéfectible de ma famille, de mes collègues et de mes amis proches, dont les encouragements, la confiance et la foi en mon travail m'ont donné la force et la détermination nécessaires pour mener à terme ce parcours.

Contents

<i>List of Figures</i>	7
<i>List of Tables</i>	8
1 Introduction	9
1.1 Overview of DoA estimation	9
1.2 Background and motivation	9
2 Signal model	12
2.1 Signal model for physical array	13
2.1.1 Ideal array	13
2.1.2 Array imperfections	14
2.2 Signal model for virtual array	15
3 Virtual array	18
3.1 Virtual linear array	18
3.2 Virtual two-dimensional array	20
3.2.1 Virtual circular array	20
3.2.2 Virtual two-dimensional rectangular lattice array	21
4 Methods	23
4.1 Bartlett beamforming	23
4.2 Capon beamforming	24
4.3 Multiple signal classification	24
4.4 Resolution performance	25
4.4.1 Ideal array	25
4.4.2 Array imperfections	26
5 Array optimization	28
5.1 Linear array optimization	28
5.1.1 Acquisition optimization	28
5.1.2 DoF optimization	29
5.2 Two-dimensional array optimization	31
5.2.1 Acquisition optimization	31
5.2.2 Number of antennas optimization	32

6 Simulation and results	34
6.1 Evaluate the performance of the virtual array	34
6.1.1 MUSIC spectra	34
6.1.2 RMSE versus SNR and snapshots	35
6.1.3 RMSE versus DoF enhancement	36
6.2 Resolution performance	37
6.3 Optimization results	38
6.3.1 Linear array	38
6.3.2 Two-dimensional array	39
7 Experiment	41
7.1 Hardware setup	41
7.2 Experimental setup	42
7.2.1 Phase calibration	42
7.2.2 Experimental challenges	42
7.3 Results	44
8 Conclusion	45
8.1 Summary of contributions	45
8.2 Perspectives	46
<i>References</i>	47
A Experimental results	51

List of Figures

1.1	Examples of moving arrays.	10
2.1	Illustration of the source positions in the far-field, in Cartesian coordinates.	12
3.1	Illustration of possible solutions with $\tilde{N}_r = 6$ and $N_r = 2$.	20
3.2	Illustration of a virtual UCA with $\tilde{N}_r = 12$.	20
4.1	Evaluation of the resolution probability of DoA estimation methods.	26
4.2	Evaluation of the resolution probability under array imperfections.	26
6.1	Virtual array MUSIC spectrum, $N_r = 2$, $L = 14$, SNR = 0 dB.	34
6.2	RMSE versus SNR for conventional MUSIC on a 12-element physical array and D-MUSIC on a 2-element virtual array, with $P = 1000$, $L = 11$.	35
6.3	RMSE versus P for conventional MUSIC on a 12-element physical array and D-MUSIC on a 2-element virtual array, with SNR = 20 dB.	36
6.4	RMSE versus DoF of virtual ULAs.	36
6.5	Evaluation of the resolution probability of DoA estimation methods.	37
6.6	Minimum solution of L obtained using the CPLEX solver for $\tilde{N}_r = 8$.	38
6.7	Solutions obtained using the CPLEX solver.	38
6.8	Comparison between existing DoF-enhanced array structures and the optimal structure obtained by the CPLEX solver.	39
6.9	Solutions obtained using the CPLEX solver.	39
7.1	USRP experiment hardware.	41
7.2	Diagram of the actual experimental setup.	43
7.3	Virtual uniform linear array.	43
7.4	Experiment results.	44

List of Tables

A.1 DoA estimation results using MUSIC for a single source.	51
---	----

Chapter 1

Introduction

1.1 Overview of DoA estimation

Direction-of-Arrival (DoA) estimation is an important application of array signal processing that has received increasing interest in the past decades. DoA estimation determines the incident directions of signal sources with respect to a sensor array. It is widely used in radio frequency and acoustics domains with similar array design and processing concepts. The performance and accuracy of the estimation algorithms are usually affected by some factors such as the coherence of sources, distribution of noise, signal-to-noise ratio (SNR), and the geometry of the sensor array. DoA estimation has proved useful in applications like sonar and radar [1]. It is also finding many applications in new generations of wireless communications and multiple input multiple output (MIMO) systems [2–4].

When the number of sources N_t is known a priori and the sources are uncorrelated, the covariance matrix of the received signal is full-rank. Classical methods, such as Bartlett [5] and Capon beamforming [6], as well as MUSIC [7], utilize the covariance matrix to construct a pseudo-spectrum, where the DoAs are determined by the N_t most dominant peaks in this spectrum. When classical methods are applied directly without considering the array geometry, the maximum number of detectable peaks is smaller than the rank of the covariance matrix, i.e., the number of sensors in the array.

1.2 Background and motivation

In this thesis, we consider the scenario where the sources are uncorrelated, far-field, non-polarized, stationary, and fixed during the signal acquisition process. Assuming that the number of sources N_t is known a priori, and that all sources operate at the same, known frequency f . Additionally, it is assumed that the relative height of the sources with respect to the array is much smaller than the distance between them, so the elevation angles can be considered zero. The source

is considered in the far-field if it lies beyond the Fraunhofer distance, $2D^2/\lambda$, where D is the aperture of the array, and λ is the wavelength of the source [8]. If the source range is less than this limit, it is considered in the near-field. The objective of this thesis is to perform DoA estimation for N_t sources using only two antennas. Therefore, when classical methods are applied, the maximum number of detectable sources is limited to one. Consequently, a method to increase the Degrees of Freedom (DoF) of the antenna system is required.

The higher the DoF of a sensor array, the greater the maximum number of sources that can be detected and the higher the DoA estimation performance. Consequently, enhanced-DoF array configurations have been proposed to improve the estimation performance of the array [9–19]. However, the maximum DoF depends on the number of physical antennas. Therefore, these configurations are inefficient when the number of antennas is small, and in the case of two antennas, only one source can be detected at most.

Typically, a signal-receiving array collects data during a single acquisition to estimate the covariance matrix corresponding to its configuration. Furthermore, the array can be translated in space, changing its position relative to the sources, and the covariance matrix can then be estimated over multiple acquisitions. If the received signals are correlated, i.e., $s(t + \tau) \approx s(t)e^{j2\pi f\tau}$ across acquisitions, the rank of the covariance matrix can be increased by increasing the number of acquisitions [20–32]. This allows the construction of an *equivalent virtual array*, where $s(t)$ denotes the signal at time t , and τ represents the time delay between the starting points of consecutive acquisitions.

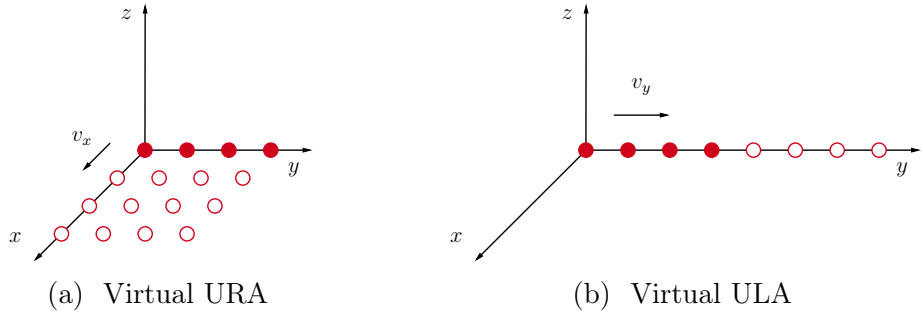


Figure 1.1: Examples of moving arrays.

Fig. 1.1 illustrates the translation of a uniform linear array (ULA) along the x - and y -axes, which correspondingly extends the array into a uniform rectangular array (URA) and increases the number of virtual antennas in the ULA.

The condition for the signals to be considered coherent is satisfied when the array translation time is much smaller than the symbol interval, i.e., $\tau \ll T_{\text{sym}}$. Simultaneously, the spacing between the virtual antennas generated by the translation should be on the order of the wavelength to enable accurate source estimation, i.e., $v\tau \approx \lambda = cT_c$, where $T_c = 1/f$. Therefore, the array velocity must

satisfy

$$v \gg v_c \triangleq \frac{cT_c}{T_{\text{sym}}}. \quad (1.1)$$

i.e., it should be much greater than the threshold velocity. Considering a narrow-band RF signal with $T_c/T_{\text{sym}} = 10^{-6}$ and $c = 3 \cdot 10^8$ m/s, the threshold velocity is $v_c = 300$ m/s. At this threshold, the required array velocity is difficult to achieve using conventional platforms. It can be observed that the existing methods for increasing the DoF are not applicable in the context of this thesis. Therefore, in the following chapter, we propose an alternative method for enhancing the DoF, which overcomes the aforementioned limitations.

Chapter 2

Signal model

Consider an array consisting of N_r identical omnidirectional physical antennas, where the position of the μ th antenna is denoted by \mathbf{r}_μ , $\mu \in \mathbb{I}_r$. The inter-element spacing is assumed to be on the order of the wavelength λ . The array receives signals from N_t sources, which are assumed to be uncorrelated, far-field, narrow-band, and stationary. The directions of the sources are characterized by unit direction vectors \mathbf{u}_i , see Fig 2.1, defined in a Cartesian coordinate system as

$$\mathbf{u}_i = (\sin \varphi_i \cos \theta_i \quad \sin \varphi_i \sin \theta_i \quad \cos \varphi_i), \quad i \in \mathbb{I}_t. \quad (2.1)$$

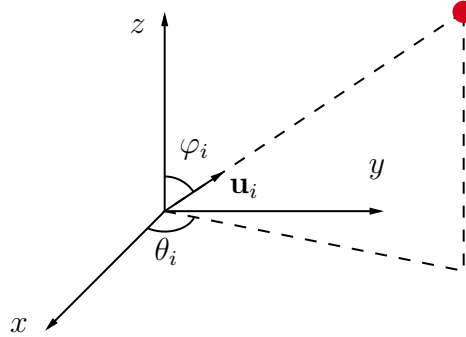


Figure 2.1: Illustration of the source positions in the far-field, in Cartesian coordinates.

Elevation angles are zero, thus $\varphi_i = \pi/2$, $\forall i \in \mathbb{I}_t$. Only distinct DOA are considered, i.e., $\theta_i \neq \theta_j$, $\forall i \neq j$, $i, j \in \mathbb{I}_t$. The array collects L acquisitions, each acquisition sampling P snapshots with a sampling interval of τ_s . The l th acquisition starts at time instant τ_l , such that

$$T_{\text{sym}} \ll P\tau_s < \tau_{l+1} - \tau_l, \quad \forall l \in \mathbb{I}_L. \quad (2.2)$$

The sources are assumed to remain non-moving throughout the L acquisitions.

The powers of the sources, denoted by σ_i^2 , $i \in \mathbb{I}_t$, are unknown. The propagation delay from the ν th antenna to the μ th antenna of the i th source is given by

$$\tau_{i,\mu} - \tau_{i,\nu} \leq \frac{\|\mathbf{r}_\mu - \mathbf{r}_\nu\|}{c} \approx \frac{\lambda}{c} = T_c \ll T_{\text{sym}}, \quad (2.3)$$

where $\tau_{i,\mu}$ is the propagation delay from the i th source to the μ th antenna. Here, we define \mathbb{I}_t , \mathbb{I}_r , \mathbb{I}_v , \mathbb{I}_p , and \mathbb{I}_L as the index sets of the sources, the physical antennas, the virtual antennas, the snapshots and the acquisitions, respectively.

2.1 Signal model for physical array

2.1.1 Ideal array

First, consider the case where the antenna positions remain fixed throughout the acquisition process, with the number of acquisitions $L = 1$. Let the acquisition start time be $\tau_1 = 0$. The signal is sampled at times $t = q\tau_s$, $q \in \mathbb{I}_p$. All antennas are assumed to be omnidirectional and free of mutual coupling, which corresponds to the ideal array model. The scalar form of the signal received at the μ th antenna is given by

$$x_\mu(t) = \sum_{i=1}^{N_t} b_i(t - \tau_{i,\mu}) e^{-j\mathbf{k}_i \cdot \mathbf{r}_\mu} + z_\mu(t), \quad \mu \in \mathbb{I}_r, \quad (2.4)$$

where $b_i(t)$ denotes the base-band signal of the i th source, and the noise at the μ th antenna is modeled as $z_\mu(t) \sim \mathcal{CN}(0, \sigma_z^2)$, and $\mathbf{k}_i = 2\pi\lambda^{-1}\mathbf{u}_i$ is the wave vector of the i th source. Due to narrow-band sources, $\tau_{i,\mu} - \tau_{i,\nu} \ll T_{\text{sym}}$. Therefore,

$$b_i(t - \tau_{i,\mu}) = b_i(t - \tau_{i,\nu}), \quad \forall \mu, \nu \in \mathbb{I}_r, \quad \forall t \in [0, P\tau_s]. \quad (2.5)$$

Approximation considered valid under the narrow-band assumption, where antenna spacing is on the order of the carrier wavelength and the sources are narrow-band. By setting $s_i(t) = b_i(t - \tau_{i,\mu})$, $\mu \in \mathbb{I}_r$, (2.4) can be rewritten as

$$x_\mu(t) = \sum_{i=1}^{N_t} s_i(t) e^{-j\mathbf{k}_i \cdot \mathbf{r}_\mu} + z_\mu(t). \quad (2.6)$$

Equation (2.6) can be expressed in matrix form as follows

$$\mathbf{x}(t) = \sum_{i=1}^{N_t} \mathbf{a}(\theta_i) s_i(t) + \mathbf{z}(t) = \mathbf{A}(\Theta) \mathbf{s}(t) + \mathbf{z}(t), \quad (2.7)$$

where $\mathbf{x}(t) \in \mathbb{C}^{N_r \times 1}$ denotes the received signal, $\mathbf{s}(t) \in \mathbb{C}^{N_t \times 1}$ contains the source signals, and $\mathbf{z}(t) \in \mathbb{C}^{N_r \times 1}$ represents the noise vector. The steering vector $\mathbf{a}(\theta_i) \in$

$\mathbb{C}^{N_r \times 1}$ is defined as

$$\mathbf{a}(\theta_i) \triangleq [e^{-j\mathbf{k}_i \cdot \mathbf{r}_1} \ e^{-j\mathbf{k}_i \cdot \mathbf{r}_2} \ \dots \ e^{-j\mathbf{k}_i \cdot \mathbf{r}_{N_r}}]^T, \quad i \in \mathbb{I}_t. \quad (2.8)$$

The steering vectors compose the steering matrix $\mathbf{A}(\Theta) \triangleq [\mathbf{a}(\theta_1) \ \dots \ \mathbf{a}(\theta_{N_t})] \in \mathbb{C}^{N_r \times N_t}$. The cross-correlation of the signals received at the μ th and ν th antennas, is given by

$$\Gamma_{\mu,\nu}(\mathbf{x}) \triangleq \mathbb{E}[x_\mu(t)x_\nu^*(t)] = \sum_{i=1}^{N_t} \sigma_i^2 e^{-j\mathbf{k}_i \cdot (\mathbf{r}_\mu - \mathbf{r}_\nu)} + \delta_{\mu,\nu} \sigma_z^2, \quad (2.9)$$

and is estimated from P snapshots as

$$\hat{\Gamma}_{\mu,\nu}(\mathbf{x}) = \frac{1}{P} \sum_{q=1}^P x_\mu(q\tau_s)x_\nu^*(q\tau_s). \quad (2.10)$$

The term $\Gamma_{\mu,\nu}(\mathbf{x})$ represents an element of the covariance matrix of the received signals. This term is time-invariant under the assumption of stationary sources. Therefore, with a sufficiently large number of snapshots, the entire covariance matrix can be estimated after a finite number of acquisitions. This property will be exploited to construct the virtual array in the subsequent chapter.

2.1.2 Array imperfections

In this section, we consider array imperfections, which include the non-omnidirectional radiation patterns of the antenna elements and the effects of linear mutual coupling. First, consider the case where all directional antennas are identical, mutual coupling is absent, and the sources are located in the far-field. In this scenario, the complex response depends on the DoA. The received signal can be expressed as

$$x_\mu(t) = \sum_{i=1}^{N_t} \rho(\theta_i) s_i(t) e^{-j\mathbf{k}_i \cdot \mathbf{r}_\mu} + z_\mu(t), \quad (2.11)$$

where $\rho(\theta_i)$ denotes the antenna response in the direction \mathbf{u}_i . By rewriting equation (2.11) in matrix form, we obtain

$$\mathbf{x}(t) = \sum_{i=1}^{N_t} \rho(\theta_i) \mathbf{a}(\theta_i) s_i(t) + \mathbf{z}(t). \quad (2.12)$$

When there is linear mutual coupling between antennas, the signal received at the μ th antenna is a linear combination of the signals received by all antennas in the

array, given by

$$x_\mu(t) = \sum_{\varrho=1}^{N_r} \beta_{\mu,\varrho} \sum_{i=1}^{N_t} \rho(\theta_i) s_i(t) e^{-j\mathbf{k}_i \cdot \mathbf{r}_\varrho} + z_\mu(t), \quad (2.13)$$

where $\beta_{\mu,\nu}$ denotes the coupling coefficient from the ν th antenna to the μ th antenna. The above expression can be rewritten in matrix form

$$\mathbf{x}(t) = \sum_{i=1}^{N_t} \tilde{\mathbf{a}}(\theta_i) s_i(t) + \mathbf{z}(t) = \tilde{\mathbf{A}}(\Theta) \mathbf{s}(t) + \mathbf{z}(t), \quad (2.14)$$

where $\tilde{\mathbf{A}}(\Theta) \triangleq \boldsymbol{\beta} \mathbf{A}(\Theta) \boldsymbol{\rho}(\Theta) \in \mathbb{C}^{N_r \times N_t}$ denotes the effective steering matrix, corresponding to the effective steering vector

$$\tilde{\mathbf{a}}(\theta) \triangleq \boldsymbol{\beta} \rho(\theta) \mathbf{a}(\theta), \quad (2.15)$$

where $\boldsymbol{\beta} = [\beta_{\mu,\nu}] \in \mathbb{C}^{N_r \times N_r}$, $\mu, \nu \in \mathbb{I}_r$ is the mutual coupling matrix, and the diagonal antenna response matrix $\boldsymbol{\rho}(\Theta) = \text{diag}(\rho(\theta_1), \dots, \rho(\theta_{N_t})) \in \mathbb{C}^{N_r \times N_r}$.

The cross-correlation term between the μ th and ν th antennas is given by

$$\Gamma_{\mu,\nu}(\mathbf{x}) = \sum_{i=1}^{N_t} \sum_{\varrho=1}^{N_r} \sum_{\varphi=1}^{N_r} \beta_{\mu,\varrho} \beta_{\nu,\varphi}^* |\rho(\theta_i)|^2 \sigma_i^2 e^{-j\mathbf{k}_i \cdot (\mathbf{r}_\varrho - \mathbf{r}_\varphi)} + \delta_{\mu,\nu} \sigma_z^2. \quad (2.16)$$

In the absence of mutual coupling, the coupling coefficients satisfy $\beta_{\mu,\varrho} \beta_{\nu,\varphi}^* = \delta_{\mu,\varrho} \delta_{\nu,\varphi}$, $\forall \mu, \varrho, \nu, \varphi \in \mathbb{I}_r$. Under this condition, equation (2.16) reduces to

$$\Gamma_{\mu,\nu}(\mathbf{x}) = \sum_{i=1}^{N_t} |\rho(\theta_i)|^2 \sigma_i^2 e^{-j\mathbf{k}_i \cdot (\mathbf{r}_\mu - \mathbf{r}_\nu)} + \delta_{\mu,\nu} \sigma_z^2. \quad (2.17)$$

For omnidirectional antennas, the antenna response satisfies $\rho(\theta) \equiv 1$, $\forall \theta \in [0, 2\pi]$. Under this condition, (2.17) reduces to (2.9).

2.2 Signal model for virtual array

First, we consider the case of an array consisting of N_r physical antennas, which are assumed to be omnidirectional and free of mutual coupling. The DoA estimation is performed using an equivalent virtual array with an arbitrary, but known, geometric configuration, where the positions of the virtual antennas are assumed to be known a priori. Classical DoA estimation methods will be employed [5–7], which require the covariance matrix of the virtual array to be estimated. In particular, this involves estimating the cross-correlation terms between the virtual

antennas.

We observe that the cross-correlation terms in (2.9) depend only on the relative positions of the antennas. Therefore, in each acquisition, the positions of the physical antennas are varied in order to sequentially estimate these terms. At the l th acquisition, the positions of the μ th and ν th antennas are given by

$$\begin{cases} \mathbf{r}_\mu(t + \tau_l) = \tilde{\mathbf{r}}_m \\ \mathbf{r}_\nu(t + \tau_l) = \tilde{\mathbf{r}}_n \end{cases} \quad \forall t \in [0, P\tau_s], \quad \forall l \in \mathbb{I}_L, \quad m, n \in \mathbb{I}_v. \quad (2.18)$$

The scalar form of the signal received at the μ th and ν antenna at the time t during the l th acquisition is given by

$$x_\mu(t + \tau_l) = \sum_{i=1}^{N_t} s_i(t + \tau_l) e^{-j\mathbf{k}_i \cdot \mathbf{r}_\mu(t + \tau_l)} + z_\mu(t + \tau_l) = \sum_{i=1}^{N_t} s_i(t + \tau_l) e^{-j\mathbf{k}_i \cdot \tilde{\mathbf{r}}_m} + z_\mu(t + \tau_l), \quad (2.19)$$

and

$$x_\nu(t + \tau_l) = \sum_{i=1}^{N_t} s_i(t + \tau_l) e^{-j\mathbf{k}_i \cdot \mathbf{r}_\nu(t + \tau_l)} + z_\nu(t + \tau_l) = \sum_{i=1}^{N_t} s_i(t + \tau_l) e^{-j\mathbf{k}_i \cdot \tilde{\mathbf{r}}_n} + z_\nu(t + \tau_l), \quad (2.20)$$

It should be noted that the assumption $s_i(t + \tau_l) = s_i(t) e^{j2\pi f \tau_l}$ is not employed here. However, since the sources are stationary, the cross-correlation between the signals remains time-invariant, which allows the covariance matrix of the virtual array to be constructed.

The cross-correlation between the two physical antennas μ and ν is equivalent to the cross-correlation between the two corresponding virtual antennas m and n ,

$$\Gamma_{m,n}(\mathbf{x}_v) \triangleq \Gamma_{\mu,\nu}(\mathbf{x}) = \sum_{i=1}^{N_t} \sigma_i^2 e^{-j\mathbf{k}_i \cdot (\tilde{\mathbf{r}}_m - \tilde{\mathbf{r}}_n)} + \delta_{\mu,\nu} \delta_{m,n} \sigma_z^2. \quad (2.21)$$

This term is estimated over P snapshots.

$$\hat{\Gamma}_{m,n}(\mathbf{x}_v) = \frac{1}{P} \sum_{q=1}^P x_\mu(q\tau_s + \tau_l) x_\nu^*(q\tau_s + \tau_l). \quad (2.22)$$

Once all pairs $(m, n) \in \mathbb{I}_v^2$ have been estimated, the covariance matrix of the equivalent virtual array can be constructed. The difference position sets of the virtual and physical arrays are respectively defined as

$$\mathbb{D}_v = \{\tilde{\mathbf{r}}_m - \tilde{\mathbf{r}}_n \mid \forall m, n \in \mathbb{I}_v\} \quad \text{and} \quad \mathbb{D}_r = \{\mathbf{r}_\mu(\tau_l) - \mathbf{r}_\nu(\tau_l) \mid \forall \mu, \nu \in \mathbb{I}_r, \forall l \in \mathbb{I}_L\}. \quad (2.23)$$

Thus, in order to construct the equivalent virtual array, it is required that $\mathbb{D}_v \subseteq \mathbb{D}_r$. Under the far-field approximation, when all antennas have identical responses

$\rho(\theta)$, (2.21) becomes

$$\Gamma_{m,n}(\mathbf{x}_v) = \sum_{i=1}^{N_t} |\rho(\theta_i)|^2 \sigma_i^2 e^{-j\mathbf{k}_i \cdot (\tilde{\mathbf{r}}_m - \tilde{\mathbf{r}}_n)} + \delta_{\mu,\nu} \delta_{m,n} \sigma_z^2. \quad (2.24)$$

This term depends only on the relative positions of the antennas. Therefore, an equivalent virtual array can also be constructed in the case of antennas with non-omnidirectional responses.

In the presence of mutual coupling between antennas, it should be noted that the terms $\beta_{\mu,\varrho} \beta_{\nu,\varphi}^*$ depend on the configuration of the antenna array. When the positions of the physical antennas are changed in each acquisition, the array configuration also changes. Therefore, an equivalent virtual array can only be constructed if the effects of mutual coupling are negligible, i.e.,

$$|\beta_{\mu,\varrho} \beta_{\nu,\varphi}^* - \delta_{\mu,\varrho} \delta_{\nu,\varphi}| \ll 1, \quad \forall \mu, \varrho, \nu, \varphi \in \mathbb{I}_r. \quad (2.25)$$

From (2.24), it can be readily verified that

$$\begin{cases} \Gamma_{n,m}(\mathbf{x}_v) = \Gamma_{m,n}^*(\mathbf{x}_v) \\ \Gamma_{m,m}(\mathbf{x}_v) = \Gamma_{n,n}(\mathbf{x}_v) \end{cases} \quad \forall m, n \in \mathbb{I}_v. \quad (2.26)$$

Thus, during the estimation of the covariance matrix, only the terms in the upper triangular part are of interest, and the auto-correlation terms need to be estimated only once. For \tilde{N}_r virtual antennas, $\tilde{N}_r(\tilde{N}_r - 1)/2$ elements of the covariance matrix need to be estimated. For $N_r \geq 2$ physical antennas, at each acquisition, at most $N_r(N_r - 1)/2$ distinct terms in the upper triangular part of the covariance matrix, excluding diagonal, can be estimated. Therefore, the number of acquisitions required to construct the array satisfying

$$\frac{\tilde{N}_r(\tilde{N}_r - 1)}{N_r(N_r - 1)} \leq L \leq \frac{\tilde{N}_r(\tilde{N}_r - 1)}{2}, \quad L \in \mathbb{N}. \quad (2.27)$$

It can be observed that the number of acquisitions required satisfies $\mathcal{O}(\tilde{N}_r^2)$. The inequality (2.27) holds for arrays with arbitrary geometric configurations. In the case of specific array structures, these upper and lower bounds can be reduced; for instance, for a ULA, the required number of acquisitions scales as $\mathcal{O}(\tilde{N}_r)$. A detailed investigation of this will be provided in a subsequent chapter. However, it is clear that minimizing the number of acquisitions requires an appropriate placement of the physical antennas. When the number of physical antennas satisfies, no explicit configuration achieves a number of acquisitions close to the lower bound; this issue will be discussed in more detail in a later chapter.

Chapter 3

Virtual array

In this chapter, the construction of three classical virtual arrays, namely the ULA, the UCA, and the URA, is considered. In this case, the scenario with $N_r = 2$ physical antennas is considered, where the antennas are ideal, omnidirectional, and there is no mutual coupling.

3.1 Virtual linear array

Consider a virtual ULA consisting of \tilde{N}_r virtual antennas. The positions of the virtual antennas can be uniquely determined by a single coordinate. Normalizing the inter-antenna spacing to $a = 1$, the positions of the virtual antennas are represented by integers.

$$\mathbb{D}_v = \{(m \ 0 \ 0)^T \mid \forall m \in \mathbb{Z}, |m| < \tilde{N}_r\}. \quad (3.1)$$

Note that the covariance matrix of a ULA is a Hermitian Toeplitz matrix. Therefore, it is sufficient to estimate only $\tilde{N}_r - 1$ elements of any row, excluding the main diagonal. The elements on the main diagonal can be determined from any acquisition, for example, the first acquisition. Thus, the number of acquisitions required to construct the virtual ULA satisfies

$$\frac{2(\tilde{N}_r - 1)}{N_r(N_r - 1)} \leq L \leq \tilde{N}_r - 1, \quad L \in \mathbb{N}. \quad (3.2)$$

We will show a mapping that represents how to construct a one-dimensional virtual array through a two-dimensional sequence. Define a two-dimensional sequence $(\alpha_{m,l})$ to represent the antenna positions at each acquisition as follows

$$\alpha_{m,l} = \begin{cases} 1 & \text{if } \exists \mu \in \mathbb{I}_r : \mathbf{r}_\mu(\tau_l) = (m \ 0 \ 0)^T, \ m \in \mathbb{I}_v, l \in \mathbb{I}_L \\ 0 & \text{otherwise.} \end{cases} \quad (3.3)$$

Since we only need to consider the positive coordinates in \mathbb{D}_v , and the covariance matrix is Hermitian, it is sufficient to consider $m \in \mathbb{I}_v$. Clearly, the construction is completely determined by $(\alpha_{m,l})$. Consider the sequence of weight functions (ω_n) , defined by

$$\omega_n \triangleq \sum_{m=-\infty}^{\infty} \sum_{l=1}^L \alpha_{m,l} \alpha_{m+n,l}. \quad (3.4)$$

Note that when $\omega_n > 0$, it implies that $(n \ 0 \ 0) \in \mathbb{D}_v \cup \mathbb{D}_r$. Moreover, $\omega_n = \omega_{-n}$ for all $n \in \mathbb{Z}$, and $\omega_0 > 0$. Therefore, to realize a virtual ULA consisting of \tilde{N}_r antennas, it is required that

$$\vartheta_{\tilde{N}_r-1} > 0, \quad \vartheta_m \triangleq \prod_{n=1}^m \omega_n > 0. \quad (3.5)$$

The DoF of a one-dimensional array is defined as the longest consecutive sequence of positive weights, given by

$$\text{DoF}_1 \triangleq \max_m \{ 2m + 1 \mid \vartheta_m > 0 \}. \quad (3.6)$$

Clearly, for a virtual ULA with \tilde{N}_r elements, we have $\text{DoF}_1 = 2\tilde{N}_r - 1$. When the array has N_r physical antennas, each acquisition allows us to estimate at most $N_r(N_r - 1)/2$ distinct cross-correlation terms, that is,

$$1 + 2L \leq \text{DoF}_1 \leq 1 + N_r(N_r - 1)L. \quad (3.7)$$

For $N_r = 2$, one can verify that

$$\alpha_{m,l} = \begin{cases} 1 & \text{if } m = 1 \\ 1 & \text{if } m = l + 1, \quad \forall l \in \mathbb{I}_L \\ 0 & \text{otherwise.} \end{cases} \quad (3.8)$$

which simultaneously satisfies the lower bound (3.2) and $\text{DoF}_1 = 2\tilde{N}_r - 1$. The virtual array achieves $\text{DoF} = 1 + 2L$, which is not upper-bounded by the number of physical antennas. For the case $N_r = 2$, a method to construct a virtual ULA is proposed, as shown in Fig. 3.1. Fig. 3.1 illustrates feasible solutions for the case $\tilde{N}_r = 6$ and $N_r = 2$ physical antennas. If $(\alpha_{m,l})$ is a solution, then any acquisition-wise permutation, also yields a valid solution. This property can be exploited to optimize the antenna configuration based on a given solution.

Consider the case where the ULA is aligned along the y -axis. From the cross-correlation terms, the covariance matrix \mathbf{R}_v , $\text{rank}(\mathbf{R}_v) = \tilde{N}_r$ of the virtual array can be estimated, with the corresponding steering vector given by

$$\mathbf{a}_v(\theta) = [e^{j\phi_1} \ \dots \ e^{j\phi_{\tilde{N}_r}}]^T, \quad (3.9)$$

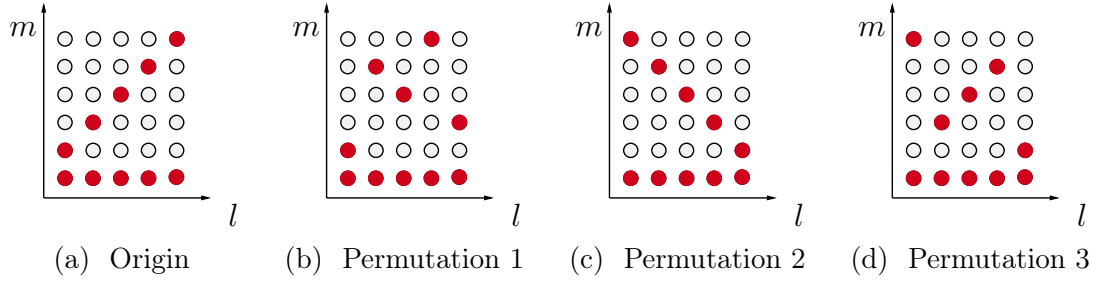


Figure 3.1: Illustration of possible solutions with $\tilde{N}_r = 6$ and $N_r = 2$.

where $\phi_i = 2\pi a(i-1) \sin \theta / \lambda$, $i \in \mathbb{I}_t$, the elements of the covariance matrix are estimated as $[\hat{\mathbf{R}}_v]_{m,n} = \hat{\Gamma}_{m,n}(\mathbf{x}_v)$, $\forall m, n \in \mathbb{I}_v$. Here, a denotes the inter-antenna spacing; in the following chapters, we set $a = \lambda/2$.

3.2 Virtual two-dimensional array

3.2.1 Virtual circular array

In the case of a virtual UCA with \tilde{N}_r virtual antennas, only the scenario with $N_r = 2$ physical antennas is considered. With an appropriate coordinate system, the position of the m th virtual antenna is given by

$$\tilde{\mathbf{r}}_m = (r \cos \xi_m \quad r \sin \xi_m \quad 0)^T \quad \forall m \in \mathbb{I}_v, \quad \xi_m = \frac{2\pi(m-1)}{\tilde{N}_r}, \quad (3.10)$$

where r is the radius of the UCA, see Fig 3.2.

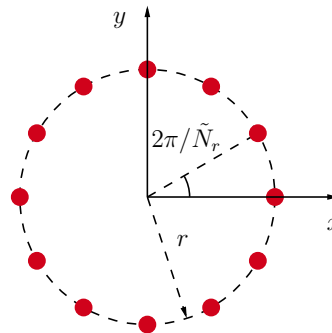


Figure 3.2: Illustration of a virtual UCA with $\tilde{N}_r = 12$.

We use the two-dimensional sequence $(\gamma_{m,n})$ to map the construction of a virtual UCA, in the case of two physical antennas. At the l th acquisition, estimating $\Gamma_{m,n}(\mathbf{x}_v)$ is equivalent to assigning $\gamma_{m,n} = l$. Assigning $(\gamma_{m,n})$ according to

increasing order of m , and then n , i.e.,

$$\gamma_{m,n} = (m-1)\tilde{N}_r + n - \frac{m(m+1)}{2} = l \quad \forall m < n, \quad m, n \in \mathbb{I}_v. \quad (3.11)$$

Thus, pure rotation can be used to vary the antenna configuration across acquisitions. From the cross-correlation terms, the covariance matrix \mathbf{R}_v , $\text{rank}(\mathbf{R}_v) = \tilde{N}_r$ of the virtual array can be estimated, with the corresponding steering vector given by

$$\mathbf{a}_v(\theta) = [e^{j\phi_1} \quad \dots \quad e^{j\phi_{\tilde{N}_r}}]^T, \quad (3.12)$$

where $\phi_i = 2\pi r \cos(\theta - \xi_i)/\lambda$, $i \in \mathbb{I}_v$. In the following sections, we choose $r = \lambda/8 \sin^2(\pi/\tilde{N}_r)$, as in [33], to avoid unambiguous angle estimates.

3.2.2 Virtual two-dimensional rectangular lattice array

Consider a two-dimensional virtual lattice array, whose set of normalized difference antenna positions is given by

$$\mathbb{D}_v = \left\{ (m \quad n \quad 0)^T \mid m \in \mathbb{I}_x, \quad v \in \mathbb{I}_y \right\}, \quad (3.13)$$

where \mathbb{I}_x and \mathbb{I}_y are the index sets along the x - and y -axes, respectively, defined as

$$\mathbb{I}_x = \{x \mid x \in \mathbb{Z}, |x| < M\} \quad \text{and} \quad \mathbb{I}_y = \{y \mid y \in \mathbb{Z}, |y| < N\}. \quad (3.14)$$

Similar to the one-dimensional array, we extend the representation to construct a two-dimensional virtual lattice array by means of the three-dimensional sequence $(\alpha_{m,n,l})$,

$$\alpha_{m,n,l} = \begin{cases} 1 & \text{if } \exists \mu \in \mathbb{I}_r, \quad l \in \mathbb{I}_L : \quad \mathbf{r}_\mu(\tau_l) = (m \quad n \quad 0)^T \\ 0 & \text{otherwise.} \end{cases} \quad (3.15)$$

For the two-dimensional array, we introduce the sequence of two-dimensional weight functions $(\omega_{m,n})$, given by

$$\omega_{m,n} \triangleq \sum_{m=-\infty}^{\infty} \sum_{n=-\infty}^{\infty} \sum_{l=1}^L \alpha_{u,v,l} \alpha_{u+m,v+n,l}. \quad (3.16)$$

Note that, for all $(m, n) \in \mathbb{Z}^2$, we have $\omega_{m,n} = \omega_{-m,-n}$ and $\omega_{0,0} > 0$. Therefore, to realize a virtual URA of size $M \times N$, it is required that

$$\vartheta_{M-1,N-1} > 0, \quad \vartheta_{m,n} \triangleq \prod_{u=-M+1}^m \prod_{v=0}^n \omega_{u,v}. \quad (3.17)$$

The DoF of the two-dimensional array is defined as the longest consecutive sequence of positive two-dimensional weight functions, given by

$$\text{DoF}_2 \triangleq \max_{m,n} \{(2m+1)(2n+1) \mid \vartheta_{m,n} > 0\}. \quad (3.18)$$

Clearly, for a virtual $M \times N$ URA, we have $\text{DoF}_2 = (2M-1)(2N-1)$. In the following chapters, unless otherwise specified, we focus on the case $M = N$. Moreover, from (3.17), it follows that $(2M-1)N-1$ cross-correlation terms need to be estimated, since $\omega_{0,0}$ corresponds to the weight of the auto-correlation term. Hence, the required number of acquisitions satisfies

$$\frac{2[N(2M-1)-1]}{N_r(N_r-1)} \leq L \leq 2(MN-1), \quad L \in \mathbb{N}. \quad (3.19)$$

When the array has N_r physical antennas, after L acquisitions one can estimate at most one auto-correlation term and $LN_r(N_r-1)/2$ distinct cross-correlation terms. The DoF of the constructed two-dimensional array is then evaluated by setting $N(2M-1) = 1 + LN_r(N_r-1)/2$, thus $\text{DoF}_2 = (2M-1)(2N-1) \leq 1 + LN_r(N_r-1)$. Once the covariance matrix of the virtual URA has been estimated, the corresponding steering vector of the virtual URA is given by $\mathbf{a}_v(\theta) \triangleq \mathbf{b}_x(\theta) \otimes \mathbf{b}_y(\theta)$, where

$$\begin{aligned} \mathbf{b}_x(\theta) &\triangleq [e^{j\phi_{x,1}} \dots e^{j\phi_{x,M}}]^T, \\ \mathbf{b}_y(\theta) &\triangleq [e^{j\phi_{y,1}} \dots e^{j\phi_{y,N}}]^T, \end{aligned} \quad (3.20)$$

with $\phi_{x,u} = 2\pi a(u-1) \cos \theta / \lambda$, $\phi_{y,v} = 2\pi(v-1) \sin \theta / \lambda$, $a = \lambda/2$ denotes the inter-element spacing, \otimes denotes the Kronecker product.

Chapter 4

Methods

Covariance-based DoA estimation methods are considered for the signal model described in (2.7), (2.14), including the Bartlett beamforming, Capon beamforming (MVDR), and MUSIC algorithm. The pseudo-spectrum $\mathcal{P}(\theta)$ is constructed over the angular domain under the assumption that the number of sources is known. The DoAs of the N_t sources correspond to the N_t dominant peaks in $\mathcal{P}(\theta)$.

4.1 Bartlett beamforming

Bartlett beamforming estimates the spatial power spectrum by computing the output power of a phased array steered in direction θ using a fixed weight vector $\omega \in \mathbb{C}^{N_r \times 1}$. The output of the array is given by

$$y(t) = \omega^H \mathbf{x}(t), \quad (4.1)$$

weight vector ω_{opt} for maximizing the array output

$$\begin{aligned} & \underset{\omega}{\text{maximize}} \quad \mathbb{E}[\|\omega^H \mathbf{x}(t)\|^2] \\ & \text{subject to} \quad \|\omega\| = 1. \end{aligned} \quad (4.2)$$

The constraint $\|\omega\| = 1$ ensures that (4.2) does not diverge. Using matrix norm inequalities, it can be shown that

$$\mathbb{E} [\|\omega^H \mathbf{x}(t)\|^2] = \mathbb{E} [|s(t)|^2 \|\omega^H \mathbf{a}(\theta)\|^2 + \sigma_z^2 \|\omega\|^2] \leq \mathbb{E} [|s(t)|^2 \|\mathbf{a}(\theta)\|^2 + \sigma_z^2]. \quad (4.3)$$

The optimal solution of (4.2) is given by

$$\omega = \frac{\mathbf{a}(\theta)}{\sqrt{\mathbf{a}^H(\theta) \mathbf{a}(\theta)}}. \quad (4.4)$$

The output power spectrum can be expressed as

$$\mathcal{P}_{\text{CB}}(\theta) = \mathbb{E} [\|\boldsymbol{\omega}^H \mathbf{x}(t)\|^2] = \frac{\mathbf{a}^H(\theta) \mathbf{R} \mathbf{a}(\theta)}{\mathbf{a}^H(\theta) \mathbf{a}(\theta)}, \quad \mathbf{R} = \mathbb{E} [\mathbf{x}(t) \mathbf{x}^H(t)]. \quad (4.5)$$

4.2 Capon beamforming

When multiple signals are present, sidelobe leakage and mutual signal interference can introduce biases in DoA estimates obtained via conventional techniques like the Bartlett algorithm. Capon proposed designing these filters optimally, namely, a linear narrow-band filter designed to pass the desired signal undistorted, while minimizing the power from all other spatial frequency bands. Formally, the following constrained optimization problem for the weight vector $\boldsymbol{\omega} \in \mathbb{C}^{N_r \times 1}$ was suggested

$$\begin{aligned} & \underset{\boldsymbol{\omega}}{\text{minimize}} \quad \boldsymbol{\omega}^H \mathbf{R} \boldsymbol{\omega} \\ & \text{subject to} \quad \boldsymbol{\omega}^H \mathbf{a}(\theta) = 1, \end{aligned} \quad (4.6)$$

that yields the well-known MVDR filter as its solution. This minimization can be solved using the method of Lagrange multipliers. Using the method of Lagrange multipliers, we can transform the constrained optimization above into an unconstrained one. The Lagrangian function is given by

$$\mathcal{L}(\boldsymbol{\omega}, \lambda) = \boldsymbol{\omega}^H \mathbf{R} \boldsymbol{\omega} + \lambda (1 - \boldsymbol{\omega}^H \mathbf{a}(\theta)), \quad \lambda \in \mathbb{C}. \quad (4.7)$$

The optimal solution of (4.7) is given by $\boldsymbol{\omega} = \lambda \mathbf{R}^{-1} \mathbf{a}(\theta)$. Using the constraint $\boldsymbol{\omega}^H \mathbf{a}(\theta) = 1$, it follows that

$$\boldsymbol{\omega} = \frac{\mathbf{R}^{-1} \mathbf{a}(\theta)}{\mathbf{a}^H(\theta) \mathbf{R}^{-1} \mathbf{a}(\theta)}, \quad (4.8)$$

with the MVDR spectrum as

$$\mathcal{P}_{\text{MVDR}}(\theta) = \frac{1}{\mathbf{a}^H(\theta) \mathbf{R}^{-1} \mathbf{a}(\theta)}. \quad (4.9)$$

4.3 Multiple signal classification

The covariance matrix of the received signal

$$\mathbf{R} = \mathbb{E} [\mathbf{x}(t) \mathbf{x}^H(t)] = \mathbf{A}(\Theta) \mathbf{R}_s \mathbf{A}^H(\Theta) + \sigma_z^2 \mathbf{I}, \quad (4.10)$$

where $\mathbf{R}_s = \mathbb{E} [\mathbf{s}(t) \mathbf{s}^H(t)]$ represents the covariance matrix of the signal. Since the signal sources are independent of each other, \mathbf{R}_s is a full-rank matrix. Therefore,

\mathbf{R} is a non-singular matrix. With eigenvalue decomposition, \mathbf{R} can be written as

$$\mathbf{R} = \sum_{i=1}^{N_r} \lambda_i \mathbf{e}_i \mathbf{e}_i^H = \mathbf{E}_s \boldsymbol{\Lambda}_s \mathbf{E}_s^H + \mathbf{E}_n \boldsymbol{\Lambda}_n \mathbf{E}_n^H, \quad (4.11)$$

where \mathbf{e}_i denotes the eigenvector associated with the eigenvalue λ_i , $i \in \mathbb{I}_r$ of the matrix \mathbf{R} , and $\boldsymbol{\Lambda}_s$, $\boldsymbol{\Lambda}_n$ represent the eigenvalues of the signal space and noise space, respectively. Obviously, the eigenvectors of the signal space and noise space are orthogonal. Considering that the steering vectors of sound sources belong to the space spanned by the signal space, the following equation with respect to the sources steering vector $\mathbf{a}(\theta)$ can be introduced

$$\mathbf{a}^H(\theta) \mathbf{E}_n = 0. \quad (4.12)$$

Therefore, the spatial spectrum of the MUSIC method can be expressed as

$$\mathcal{P}_{\text{MUSIC}}(\theta) = \frac{1}{\mathbf{a}^H(\theta) \mathbf{E}_n \mathbf{E}_n^H \mathbf{a}(\theta)}, \quad (4.13)$$

where \mathbf{E}_n is the matrix whose columns span the subspace formed by the $N_r - N_t$ eigenvectors corresponding to the $N_r - N_t$ smallest eigenvalues. As a result, the MUSIC algorithm is capable of detecting up to $N_r - 1$ sources.

4.4 Resolution performance

In this section, we investigate the resolution capability of DoA estimation methods for a ULA through simulations, averaged over 5000 Monte Carlo runs. We consider the case of two closely spaced sources with angles of arrival θ and $\theta + \Delta\theta$. The receiver is equipped with five antennas, the number of snapshots is set to P , $\theta = 10^\circ$. Based on the resolution probability criterion, we will determine the most appropriate DoA estimation algorithm to be employed for the virtual array in the subsequent sections.

4.4.1 Ideal array

The antennas are assumed to be ideal, omnidirectional, and free from mutual coupling effects. In Fig. 4.1a, 100 snapshots are used, with a source separation of $\Delta\theta = 10^\circ$, while Fig. 4.1b corresponds to an SNR of 10 dB, 100 snapshots. In each simulation trial shown in Fig. 4.1, the two sources were considered resolved if two distinct peaks were detected and the estimation errors of both angles were less than one degree. From Figs. 4.1a and 4.1b, it can be observed that the resolution probability of MUSIC outperforms those of MVDR and Bartlett. Therefore, in the subsequent simulations, only MUSIC is employed for DoA estimation.

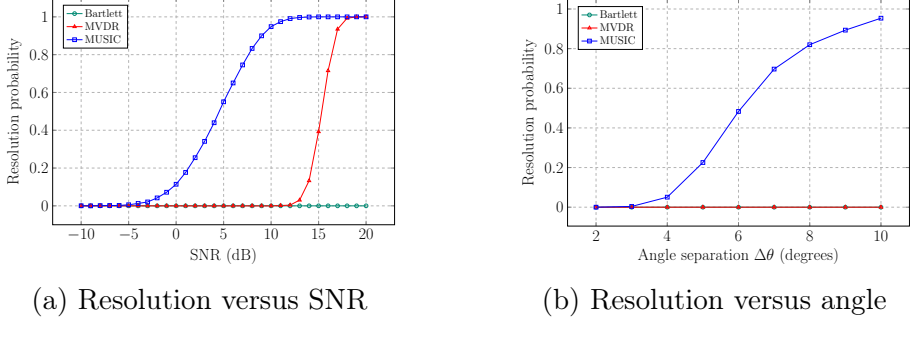


Figure 4.1: Evaluation of the resolution probability of DoA estimation methods.

4.4.2 Array imperfections

In this section, we sequentially describe two array imperfections for the ULA. The antenna response is modeled as $\rho(\theta) = e^{-\alpha_0^2 \theta^2} e^{j\alpha_1 \theta}$, we only investigate the resolution probability for a single source at different angles for this antenna response. Next, we investigate the order of magnitude of the mutual coupling coefficients as approximated in (2.25). This is done by performing DoA estimation for an omnidirectional antenna array with mutual coupling while using the steering vector $\mathbf{a}(\theta)$ of ideal antennas, and evaluating the effect through the resolution probability. The coupling matrix is assumed to be a banded structure, as in [34], and is given by

$$\beta_{\mu,\nu} = \begin{cases} \frac{\beta_0}{|\mu - \nu|} \exp\left(-j\frac{2\pi}{5}|\mu - \nu|\right), & 0 < |\mu - \nu| \leq 4 \\ 1, & \mu = \nu \\ 0, & \text{otherwise.} \end{cases} \quad (4.14)$$

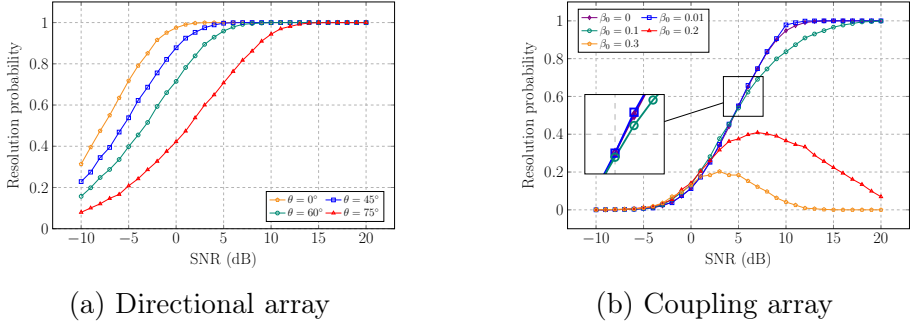


Figure 4.2: Evaluation of the resolution probability under array imperfections.

Figure 4.2 presents the resolution probability, averaged over 5000 Monte Carlo runs, in two cases, a non-omnidirectional antenna without mutual coupling, Fig. 4.2a, and an omnidirectional antenna with mutual coupling, Fig. 4.2b. Fig. 4.2a illustrates the case of non-isotropic antennas without mutual coupling,

with $\alpha_0 = 24/\pi$, $\alpha_1 = 2$, $\beta_0 = 0$. As shown in Fig. 4.2a, the magnitude of the antenna pattern is highly concentrated around 0° and rapidly decreases towards both sides, $\Delta\theta = 10^\circ$. Consequently, the resolution probability decreases significantly as the angle of arrival deviates further from 0° .

On the other hand, Fig. 4.2b indicates that when the mutual coupling coefficients are on the order of 0.1 or smaller, the effect of mutual coupling can be approximately neglected. In particular, even when using the steering vector of omnidirectional antennas, if the mutual coupling coefficient is on the order of 0.01, the resolution capability approaches that of the ideal case without mutual coupling.

Chapter 5

Array optimization

From (2.27), it follows that to construct a virtual array with \tilde{N}_r antennas in an arbitrary geometry, $\mathcal{O}(\tilde{N}_r^2)$ acquisitions are required, which grows rapidly with \tilde{N}_r . To reduce the required number of acquisitions, one could increase the number of physical antennas. However, there is no closed-form solution that allows L to approach the lower bound in (2.27). Therefore, we present a method to construct a virtual array from any N_r physical antennas and optimize the number of acquisitions. As the number of acquisitions increases, the DoF of the virtual array increases, and the maximum number of detectable sources also increases. Nevertheless, it must be ensured that the source positions remain unchanged throughout all acquisitions. In practice, sources may move after a finite time; hence, to maximize the number of detectable sources, one needs to maximize the DoF given a limited number of acquisitions. In this chapter, we model these two optimization problems as mixed-integer linear programs (MILPs), and solve them as combinatorial optimization problems.

5.1 Linear array optimization

5.1.1 Acquisition optimization

Given a virtual array with \tilde{N}_r antennas and a predetermined number of physical antennas N_r , we seek a solution $(\alpha_{m,l})$ that minimizes the number of acquisitions, while satisfying $\vartheta_{\tilde{N}_r-1} > 0$ and ensuring that the number of physical antennas in each acquisition is N_r . Therefore, the optimization problem can be formulated as

$$\begin{aligned} & \underset{L}{\text{minimize}} && L \\ & \text{subject to} && \vartheta_{\tilde{N}_r-1} > 0 \\ & && \sum_{m=1}^{\tilde{N}_r} \alpha_{m,l} = N_r, \quad \forall l \in \mathbb{I}_L. \end{aligned} \tag{5.1}$$

To formulate the problem as a MILP, the term ϱ_m needs to be linearized by introducing auxiliary variables as follows $z_{m,n,l} \triangleq \alpha_{m,l}\alpha_{m+n,l} \in \{0, 1\}$, and

$$\begin{cases} z_{m,n,l} \leq \alpha_{m,l} \\ z_{m,n,l} \leq \alpha_{m+n,l} \\ z_{m,n,l} \geq \alpha_{m,l} + \alpha_{m+n,l} - 1 \end{cases} \quad \forall m \in \mathbb{I}_r, \quad \forall l \in \mathbb{I}_L, \quad n \in \mathbb{N}, \quad n < \tilde{N}_r. \quad (5.2)$$

Since L is upper-bounded by $\mathcal{L}_1 \triangleq \tilde{N}_r - 1$, we solve (5.1) using the CPLEX solver. The solver stops as soon as it finds the first solution that satisfies all constraints. Therefore, we introduce auxiliary variables $u_l \in \{0, 1\}$, where

$$u_l = \begin{cases} 1 & \text{if } \exists m \in \mathbb{I}_v : \alpha_{m,l} = 1 \\ 0 & \text{otherwise.} \end{cases} \quad (5.3)$$

Let $v_{m,l} \triangleq u_l\alpha_{m,l} \in \{0, 1\}$, $y_{m,n,l} \triangleq u_l z_{m,n,l} = v_{m,l}\alpha_{m+n,l} \in \{0, 1\}$. The optimization problem can then be reformulated as

$$\begin{aligned} & \text{minimize} && \sum_{l=1}^{\mathcal{L}_1} u_l \\ & \text{subject to} && v_{m,l} \leq u_l \\ & && v_{m,l} \leq \alpha_{m,l} \\ & && v_{m,l} \geq u_l + \alpha_{m,l} - 1 \\ & && y_{m,n,l} \leq v_{m,l} \\ & && y_{m,n,l} \leq \alpha_{m+n,l} \\ & && y_{m,n,l} \geq v_{m,l} + \alpha_{m+n,l} - 1 \\ & && \sum_{l=1}^{\mathcal{L}_1} \sum_{m=1}^{\tilde{N}_r} y_{m,n,l} > 0, \quad \forall n \in \mathbb{N}, \quad n < \tilde{N}_r \\ & && \sum_{m=1}^{\tilde{N}_r} v_{m,l} = N_r, \quad \forall l \in \mathbb{I}_L, \quad l < \mathcal{L}_1. \end{aligned} \quad (5.4)$$

Since (5.4) does not have a closed-form solution, we solve it using the CPLEX solver on the NEOS server.

5.1.2 DoF optimization

Given the number of acquisitions L and a predetermined number of physical antennas N_r , we seek a solution $(\alpha_{m,l})$ that maximizes the DoF, while satisfying $\vartheta_{\tilde{N}_r-1} > 0$ and ensuring that the number of physical antennas in each acquisition

is N_r . Therefore, the optimization problem can be formulated as

$$\begin{aligned} & \underset{\tilde{N}_r}{\text{maximize}} \quad 2\tilde{N}_r - 1 \\ & \text{subject to} \quad \vartheta_{\tilde{N}_r-1} > 0 \\ & \quad \sum_{m=1}^{\tilde{N}_r} \alpha_{m,l} = N_r, \quad \forall l \in \mathbb{I}_L. \end{aligned} \tag{5.5}$$

Since DoF_1 is upper-bounded by $\mathcal{D}_1 \triangleq 1 + LN_r(N_r - 1)$, the optimization problem can then be reformulated as

$$\begin{aligned} & \underset{(y_n)}{\text{maximize}} \quad 1 + 2 \sum_{n=1}^{\mathcal{D}_1} y_n \\ & \text{subject to} \quad y_n \leq y_{n-1} \\ & \quad y_n \in \{0, 1\} \\ & \quad z_{m,n,l} \leq \alpha_{m,l} \\ & \quad z_{m,n,l} \leq \alpha_{m+n,l} \\ & \quad z_{m,n,l} \geq \alpha_{m,l} + \alpha_{m+n,l} - 1 \\ & \quad \sum_{m=1}^{\mathcal{D}_1} \alpha_{m,l} = N_r, \quad \forall l \in \mathbb{I}_L \\ & \quad \sum_{l=1}^L \sum_{m=1}^{\mathcal{D}_1} z_{m,n,l} \leq y_n LN_r, \quad \forall n \in \mathbb{N}^+, \quad n < \mathcal{D}_1. \end{aligned} \tag{5.6}$$

Since (5.6) does not have a closed-form solution, we also solve it using the CPLEX solver on the NEOS server. In the case of $L = 1$, the problem reduces to finding the optimal DoF configuration for a one-dimensional array given a predetermined number of physical antennas.

Observing the solutions in Fig. 3.1, we notice that, compared with the solution 3.1a and 3.1c, the solutions corresponding to 3.1b and 3.1d are less “regular”, since the total displacement required to reposition the antennas is larger. For a given solution, one can thus identify a whole family of corresponding solutions, among which the “most regular” one can be selected. Note that, if $(\alpha_{m,l})$ is a solution of (5.4) or (5.6), then the family $(\alpha_{f_k(m), \sigma(l)})_{m,l}$ also constitutes a corresponding family of solutions, where $\sigma(\cdot)$ denotes a permutation over the acquisition indices and $f_k(\cdot)$ is defined as

$$f_k(m) \triangleq a(l) + (-1)^k m, \quad k \in \{0, 1\}, \tag{5.7}$$

with $a(l)$ at each acquisition l being distinguishable, chosen such that

$$\begin{aligned} \min_m f_k(m) &\geq 1, \\ \max_m f_k(m) &\leq \min\{\mathcal{D}_1, \tilde{N}_r\}. \end{aligned} \quad (5.8)$$

5.2 Two-dimensional array optimization

5.2.1 Acquisition optimization

For the two-dimensional array case, only the *two-dimensional lattice structure* is considered. Given an $M \times N$ configuration and a predetermined number of physical antennas N_r , the objective is to determine a solution $(\alpha_{m,n,l})$ that minimizes the number of acquisitions, subject to the constraint $\vartheta_{M-1,N-1} > 0$, while ensuring that each acquisition involves exactly N_r physical antennas. The optimization problem can be formulated as

$$\begin{aligned} &\underset{L}{\text{minimize}} \quad L \\ &\text{subject to} \quad \vartheta_{M-1,N-1} > 0 \\ &\quad \sum_{n=1}^N \sum_{m=1}^M \alpha_{m,n,l} = N_r, \quad \forall l \in \mathbb{I}_L. \end{aligned} \quad (5.9)$$

Similar to the one-dimensional array case, once a solution $(\alpha_{m,n,l})$ is obtained, a family of equivalent solutions can also be derived $(\alpha_{u(m),v(n),\sigma(l)})_{m,n,l}$. However, all transformations associated with m and n must share the same constants $a_m(l)$, $a_n(l)$. This is equivalent to translating the entire solution within a finite number of acquisitions, while ensuring that it remains confined within the $M \times N$ rectangle.

$$\begin{cases} u(m) \triangleq a_m(l) + (-1)^k m & k \in \{0, 1\}, \\ v(n) \triangleq a_n(l) + (-1)^k n \end{cases} \quad (5.10)$$

the constants $a_m(l)$, $a_n(l)$ are chosen such that

$$\forall (m, n) \in [1, M] \times [1, N] : (u(m), v(n)) \in [1, M] \times [1, N]. \quad (5.11)$$

Since L is upper-bounded by $\mathcal{L}_2 \triangleq 2(MN - 1)$ (3.19), the optimization can be performed in the same manner as in the linear array case. Define the binary variables $z_{u,v,l} \triangleq u_l \alpha_{u,v,l}$, $y_{u,v,m,n,l} \triangleq u_l \alpha_{u,v,l} \alpha_{u+m,v+n,l}$. The optimization problem

can be reformulated as

$$\begin{aligned}
& \underset{(u_l)}{\text{minimize}} \quad \sum_{l=1}^{\mathcal{L}_2} u_l \\
& \text{subject to} \quad z_{u,v,l} \leq u_l \\
& \quad z_{u,v,l} \leq \alpha_{u,v,l} \\
& \quad z_{u,v,l} \geq u_l + \alpha_{u,v,l} - 1 \\
& \quad y_{u,v,m,n,l} \leq z_{u,v,l} \\
& \quad y_{u,v,m,n,l} \leq \alpha_{u+m,v+n,l} \\
& \quad y_{u,v,m,n,l} \geq z_{u,v,l} + \alpha_{u+m,v+n,l} - 1 \\
& \quad \sum_{l=1}^{\mathcal{L}_2} \sum_{v=1}^N \sum_{u=1}^M y_{u,v,m,n,l} > 0, \quad \forall (m, n) \in \mathbb{Z}^2, |m| < M, 0 \leq n < N \\
& \quad \sum_{v=1}^N \sum_{u=1}^M z_{u,v,l} = N_r, \quad \forall l \in \mathbb{N}, l < \mathcal{L}_2.
\end{aligned} \tag{5.12}$$

5.2.2 Number of antennas optimization

In this section, given a virtual array of size $M \times N$ and a finite number of acquisitions, we aim to minimize the number of physical antennas N_r . For the special case of a single acquisition $L = 1$, the optimization problem reduces to the formulation in [35]. For the general case with multiple acquisitions $L > 1$, the problem can be expressed as follows

$$\begin{aligned}
& \underset{(\alpha_{u,v,l})}{\text{minimize}} \quad \sum_{v=1}^N \sum_{u=1}^M \alpha_{u,v,1} \\
& \text{subject to} \quad \vartheta_{M-1,N-1} > 0 \\
& \quad \sum_{n=1}^N \sum_{m=1}^M \alpha_{u,v,l} = \sum_{v=1}^N \sum_{u=1}^M \alpha_{u,v,1}, \quad \forall l \in \mathbb{I}_L.
\end{aligned} \tag{5.13}$$

Here, we linearize the term $\vartheta_{m,n}$ using the auxiliary variable $y_{u,v,m,n,l} \triangleq \alpha_{u,v,l} \alpha_{u+m,v+n,l}$ and note that the number of antennas in each acquisition is constrained to be the same, i.e.,

$$\sum_{v=1}^N \sum_{u=1}^M \alpha_{u,v,l} = \sum_{v=1}^N \sum_{u=1}^M \alpha_{u,v,1}, \quad \forall l \in \mathbb{I}_L. \tag{5.14}$$

Similarly to the minimum-acquisition problem, it can be reformulated as

$$\begin{aligned}
& \underset{(\alpha_{u,v,l})}{\text{minimize}} \quad \sum_{v=1}^N \sum_{u=1}^M \alpha_{u,v,1} \\
& \text{subject to} \quad y_{u,v,m,n,l} \leq \alpha_{u,v,l} \\
& \quad y_{u,v,m,n,l} \leq \alpha_{u+m,v+n,l} \\
& \quad y_{u,v,m,n,l} \geq \alpha_{u,v,l} + \alpha_{u+m,v+n,l} - 1 \\
& \quad \sum_{l=1}^L \sum_{v=1}^N \sum_{m=1}^M y_{u,v,m,n,l} > 0, \quad \forall (m, n) \in \mathbb{Z}^2, |m| < M, 0 \leq n < N \\
& \quad \sum_{n=1}^N \sum_{m=1}^M \alpha_{u,v,l} = \sum_{v=1}^N \sum_{u=1}^M \alpha_{u,v,1}, \quad \forall l \in \mathbb{I}_L.
\end{aligned} \tag{5.15}$$

We also solve (5.12) and (5.15) using the CPLEX solver on the NEOS server.

Chapter 6

Simulation and results

6.1 Evaluate the performance of the virtual array

6.1.1 MUSIC spectra

In this section, simulations are conducted with N_t sources, whose number is assumed to be known a priori and with equal power. The noise is assumed to be spatially and temporally white. During each acquisition, the antenna array collects P snapshots. We evaluate the performance of DoA estimation using the proposed virtual arrays constructed from only two physical antennas denoted DoF-enhanced MUSIC (D-MUSIC), forming a virtual array with the same DoF. For conventional MUSIC, the sample covariance matrix is estimated using P snapshots. we also compare the proposed approach with conventional MUSIC algorithm for ULA and UCA each composed of N_r antennas

$$\hat{\mathbf{R}} = \frac{1}{P} \sum_{q=1}^P \mathbf{x}(q\tau_s) \mathbf{x}^H(q\tau_s). \quad (6.1)$$

In contrast, D-MUSIC estimates the covariance matrix using LP snapshots.

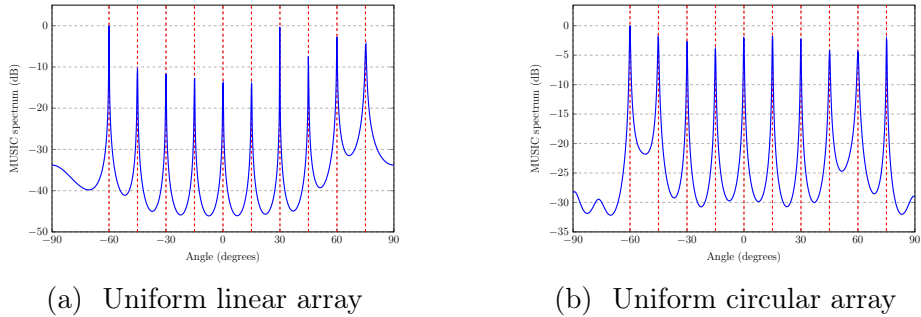


Figure 6.1: Virtual array MUSIC spectrum, $N_r = 2$, $L = 14$, SNR = 0 dB.

Fig.6.1 shows the MUSIC spectra obtained using the proposed DoF-enhancement

method, where the red dashed lines indicate the true angles of arrival. In this example, we consider 10 sources and 14 acquisitions. For such a configuration, the methods proposed in [9–19] achieve a maximum DoF = 3, thus being able to detect at most 1 source, which is insufficient for estimating the DoAs of 10 sources. Moreover, the approach in [20–32] cannot be applied in the case of RF-band signals, as previously discussed.

6.1.2 RMSE versus SNR and snapshots

In the following simulation, 8 sources impinge from directions $\theta_i \in \mathbb{A}$, $i \in \mathbb{I}_t$, where $\mathbb{A} = \{-60^\circ, -45^\circ, -30^\circ, 0^\circ, 15^\circ, 30^\circ, 45^\circ, 60^\circ\}$. The root mean square error (RMSE) of DoA estimation is compared between the conventional MUSIC algorithm with $N_r = 12$ physical antennas and the proposed virtual MUSIC approach with two physical antennas, using the DoF-enhancement technique with $\tilde{N}_r = 1 + L = 12$. Here, the RMSE of DoA estimation is defined as

$$\text{RMSE} = \left[\mathbb{E} \left(\frac{1}{N_t} \sum_{i=1}^{N_t} (\theta_i - \hat{\theta}_i)^2 \right) \right]^{1/2}, \quad (6.2)$$

where $\hat{\theta}_i$ is the DoA estimation of the i th source.

Fig. 6.2 shows the RMSE of the two methods as a function of SNR, averaged over 1500 Monte Carlo simulations, 1000 snapshots. Although the D-MUSIC method achieves the same number of DoF as conventional MUSIC, its performance is slightly inferior due to the limited number of snapshots. For the virtual array results in Fig. 6.2a and Fig. 6.2b, the RMSE difference between the two methods decreases as the SNR increases. For the virtual ULA, the RMSE difference between the two methods reaches approximately 0.07° at high SNR, which is of the same order of magnitude as the results reported in [9] under similar simulation conditions.

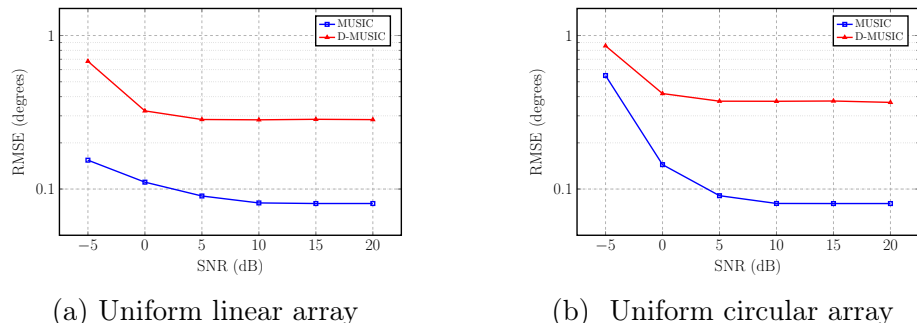


Figure 6.2: RMSE versus SNR for conventional MUSIC on a 12-element physical array and D-MUSIC on a 2-element virtual array, with $P = 1000$, $L = 11$.

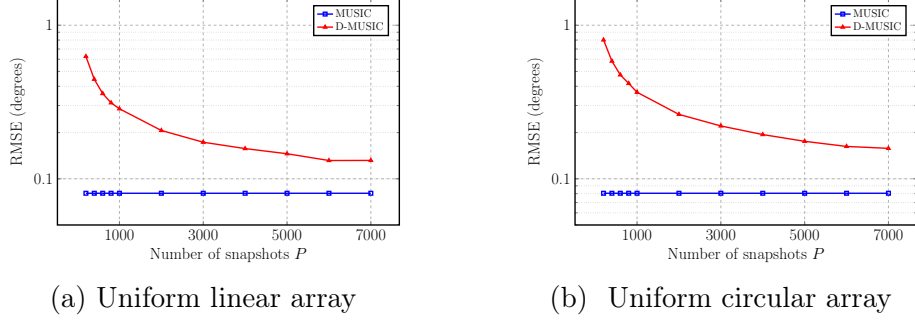


Figure 6.3: RMSE versus P for conventional MUSIC on a 12-element physical array and D-MUSIC on a 2-element virtual array, with SNR = 20 dB.

Fig. 6.3 compares the RMSE of conventional MUSIC and D-MUSIC with the same DoF as a function of the number of snapshots. As the number of snapshots increases, the RMSE of the D-MUSIC method decreases significantly and asymptotically approaches that of the conventional MUSIC.

6.1.3 RMSE versus DoF enhancement

This section presents simulations involving N_t equal-power sources received by two physical antennas. The effect of DoF enhancement through the proposed approach on the RMSE of DoA estimation is evaluated for the virtual ULA, averaged over 1500 Monte Carlo runs, with 1000 snapshots per acquisition.

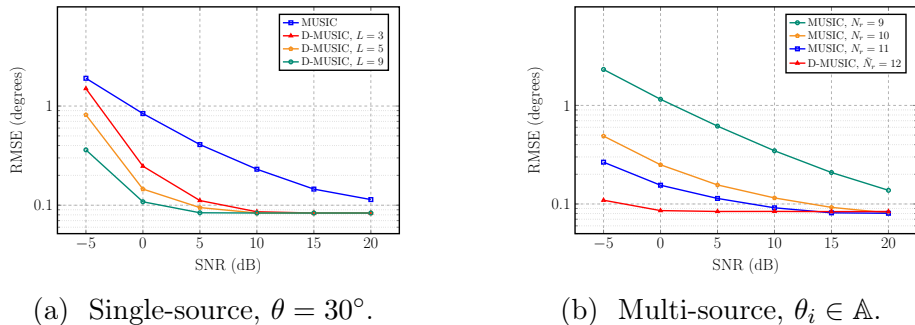


Figure 6.4: RMSE versus DoF of virtual ULAs.

As observed from Figs. 6.2a and Fig. 6.2b, the RMSE converges rapidly at high SNR levels, particularly beyond 10 dB. Furthermore, Fig. 6.4a demonstrates that increasing the number of acquisitions L , thereby enhancing the DoF as $\text{DoF} = 1 + 2L$, leads to a reduced RMSE and faster convergence. At low SNR, the RMSE decreases as L increases, with a significant reduction compared to the case of MUSIC, $L = 1$.

Fig. 6.4b illustrates the simulation results for 8 sources impinge from directions $\theta_i \in \mathbb{A}$, $i \in \mathbb{I}_t$, estimated using conventional MUSIC with $N_r \in \{9, 10, 11\}$ over P_1 snapshots, and D-MUSIC using only two physical antennas, corresponding to a

virtual array of size $\tilde{N}_r = 12$, over LP_2 snapshots, where $P_1 = 500$, $P_2 = 10^5$. After applying the proposed approach to increase the DoF, it is observed that, for the same DoF, the RMSE of D-MUSIC is higher than that of conventional MUSIC, as shown in Fig. 6.3a, Fig. 6.3b. However, at high SNR, increasing the number of snapshots leads to a reduction in the RMSE of D-MUSIC, which gradually approaches that of conventional MUSIC, while the RMSE of conventional MUSIC remains unchanged. Fig. 6.4b demonstrates that, when the number of snapshots is sufficiently large and the DoF of D-MUSIC exceeds that of conventional MUSIC, D-MUSIC achieves a lower RMSE, with only two physical antennas.

6.2 Resolution performance

In this section, the resolution performance of the virtual array is investigated for two closely spaced sources at angles θ and $\theta + \Delta\theta$, as illustrated in Fig. 6.5. Fig. 6.5a compares the resolution performance of a physical ULA with 5 antennas, whose DoAs are estimated using MUSIC, with that of the virtual arrays constructed from 2 physical antennas and estimated using D-MUSIC, based on 100 snapshots over 5000 Monte Carlo runs, $\theta = 10^\circ$, SNR = 10 dB. The physical array estimates the DoAs using MUSIC based on a covariance matrix constructed from $P = 200$ snapshots, whereas the virtual array estimates the DoAs using D-MUSIC based on a virtual covariance matrix obtained from LP snapshots. It can be observed that, for the same number of snapshots per acquisition and identical DoF, the resolution performance of MUSIC is superior to that of D-MUSIC. However, when the DoF of D-MUSIC is increased, the virtual array achieves resolution performance that outperforms MUSIC at all angles.

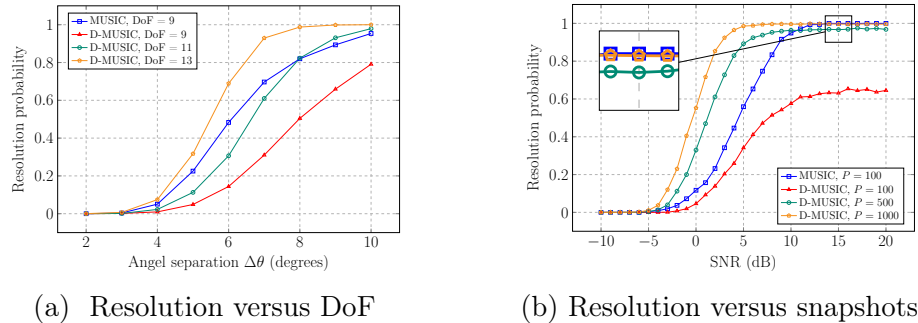


Figure 6.5: Evaluation of the resolution probability of DoA estimation methods.

It can be observed that the virtual array exhibits limited resolution performance due to the relatively small number of snapshots. Therefore, the resolution performance of this configuration is further examined by gradually increasing the number of snapshots for D-MUSIC. As shown in Fig. 6.5b, the resolution of the virtual array improves with the number of snapshots, outperforming the physical

array with the same DoF at low SNR, and approaching the performance of the physical array at high SNR.

6.3 Optimization results

6.3.1 Linear array

Fig. 6.6 shows the optimal solution obtained by the CPLEX solver for the virtual linear array with $\tilde{N}_r = 8$. From this solution, we derive a specific construction that will be used in the following analysis. It can be observed that, for all $N_r \geq 2$, the number of acquisitions achieves the lower bound $\mathcal{L}_0 \triangleq 2(\tilde{N}_r - 1)/N_r(N_r - 1)$.

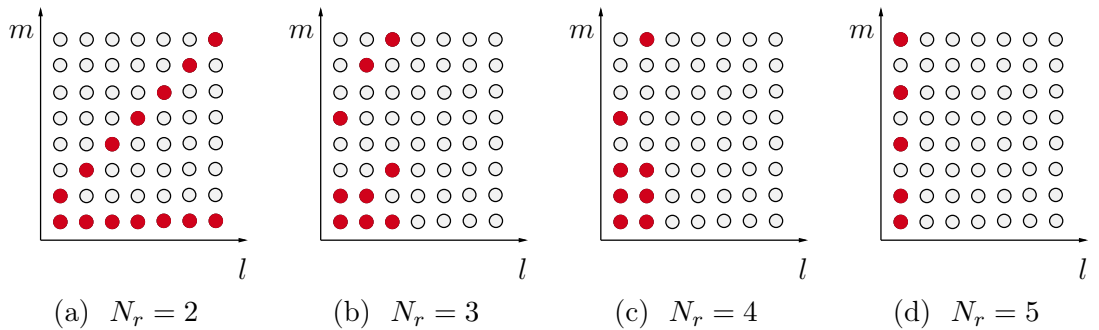


Figure 6.6: Minimum solution of L obtained using the CPLEX solver for $\tilde{N}_r = 8$.

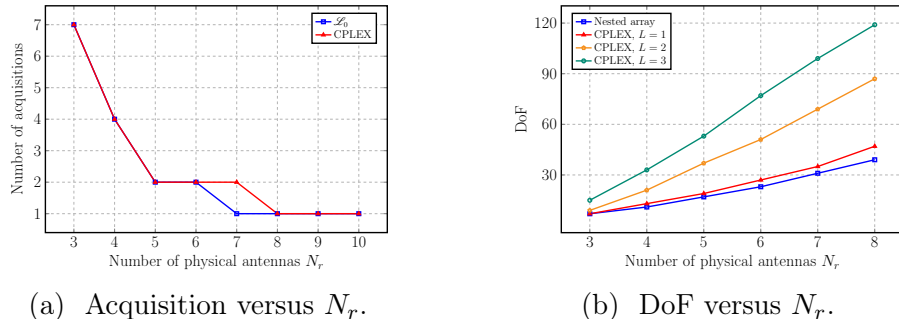


Figure 6.7: Solutions obtained using the CPLEX solver.

Fig. 6.7 shows the optimal results obtained by the CPLEX solver for determining the minimal L , compared with the theoretical lower bound \mathcal{L}_0 in (3.2). It can be observed that for the case of 20 virtual antennas, the optimal solution almost always achieves the corresponding lower bound.

When $L = 1$, this is equivalent to finding the difference coarray configuration that maximizes the DoF. In Fig. 6.7b, we compare the optimal results obtained using the CPLEX solver with those of a nested array structure. It can be observed that the solutions found by the CPLEX solver yield higher DoF than the Nested

array [9] for all given numbers of physical antennas. As L increases, the achievable DoF grow rapidly with respect to the number of physical antennas N_r .

6.3.2 Two-dimensional array

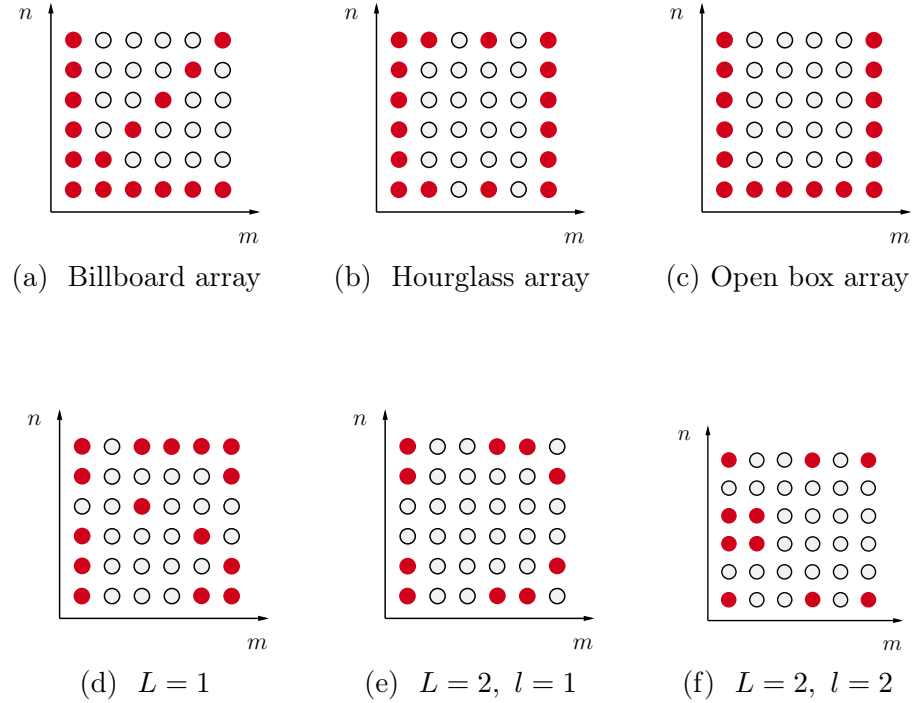


Figure 6.8: Comparison between existing DoF-enhanced array structures and the optimal structure obtained by the CPLEX solver.

It can be observed that the optimal structure obtained by the CPLEX solver requires fewer antennas than the existing DoF-enhanced array structures, and the number of antennas is significantly reduced when increasing the number of acquisitions L . Figure 6.8d shows the solution obtained by the CPLEX solver with $L = 1$, while Figures 6.8e and 6.8f present the solutions with $L = 2$, corresponding to acquisitions $l = 1$ and $l = 2$, respectively.

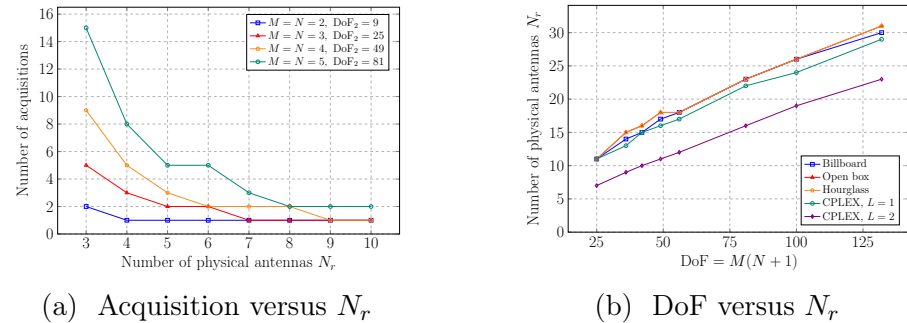


Figure 6.9: Solutions obtained using the CPLEX solver.

Figure 6.9a shows the optimal solution, corresponding to the minimal number of acquisitions for the two-dimensional array. For a two-dimensional array, the number of terms to be estimated grows rapidly; however, by employing the optimal configuration obtained from the CPLEX solver, this number is significantly reduced and decreases faster as the number of physical antennas increases.

In Fig. 6.9b, the DoF refers to the maximum number of sources with almost-sure identifiability, see [36, 37]. It can be observed that the optimal solution obtained using the CPLEX solver with $L = 1$ is consistent with [35], requiring fewer antennas than other array structures. For $L = 2$, the number of required antennas decreases significantly compared to the case of $L = 1$.

Chapter 7

Experiment

7.1 Hardware setup

In this section, we conduct DoA estimation experiments using SDR devices for signal transmission and reception. The transmission and reception are implemented in GNU Radio, while the received signals are processed in Python and MATLAB for DoA estimation.

The receiver consists of two antennas sharing the same local oscillator to avoid frequency offset between the received signals, with synchronized sampling and a low mutual coupling factor. Initially, the receiver employs the two RX1 and RX2 ports of the BladeRF for signal acquisition. As a first step, we evaluate the coupling coefficient by connecting the antenna to only one of the RX ports and observing the spectrograms of both ports. We observe that the spectrogram of the port without an antenna is correlated with that of the connected port but with approximately 10 dB attenuation. This implies a coupling coefficient of about $\beta_0 \approx 0.3$, which, according to the simulation results in Fig. 4.2b, is not suitable for practical use.



Figure 7.1: USRP experiment hardware.

We then replaced the receiver with two USRP B200 devices in order to reduce the coupling effect, while employing an external 10 MHz oscillator as a common reference. One USRP B200 was used as the transmitter to generate a sinusoidal

waveform, and the signals were acquired using GNU Radio. However, when both devices were recording simultaneously, buffer errors occurred, which affected the phase alignment of the sinusoid. Moreover, the timing of these buffer faults was uncontrollable, making this setup unsuitable for DoA estimation.

Subsequently, we switched to MATLAB for signal acquisition, which allows processing at the sample level to avoid buffer-related errors. Nevertheless, this approach required a PPS source for synchronization. When supplying the PPS signal to the receivers, MATLAB reported errors as the UHD driver failed to detect the external PPS.

As a final solution, we adopted a USRP B210 as the receiver, using its RF A and RF B ports. This configuration provides a sufficiently low coupling coefficient and ensures a shared oscillator between RF A and RF B, thereby enabling reliable signal acquisition. On the transmitter side, a USRP B200 was employed, with transmission and reception controlled using GNU Radio. The received data were subsequently processed in MATLAB for DoA estimation.

7.2 Experimental setup

This experiment was carried out with a center frequency of 446.00625 MHz. For the purpose of DoA estimation, we employed a ULA configuration with an inter-element spacing of 33.6 cm, corresponding to half a wavelength. Consequently, coaxial cables were used to connect the antennas to the RX ports of the USRP receiver.

7.2.1 Phase calibration

We denote the received signals from the two antennas as $x_1(t)$ and $x_2(t)$. DoA estimation can be biased due to phase differences arising from both antenna spacing and unequal cable lengths. To calibrate, the transmitter is connected to a 2-way splitter, whose outputs feed the two cables. The measured phase difference thus reflects only the cable mismatch, allowing us to correct $x_1(t)$. The calibrated signals $z_1(t)$ and $z_2(t)$, used for DoA estimation, are then given by

$$\begin{aligned} z_1(t) &= x_1(t)e^{-j\Delta\Phi_l}, & \Delta\Phi_l &\triangleq \mathbb{E}[\angle(x_1(t)x_2^*(t))], \\ z_2(t) &= x_2(t), \end{aligned} \tag{7.1}$$

where z_1 and z_2 denote the signals after phase calibration.

7.2.2 Experimental challenges

Fig 7.2 shows the actual experimental setup. To ensure far-field conditions, the transmitters were placed more than 30 wavelengths away from the receivers. With

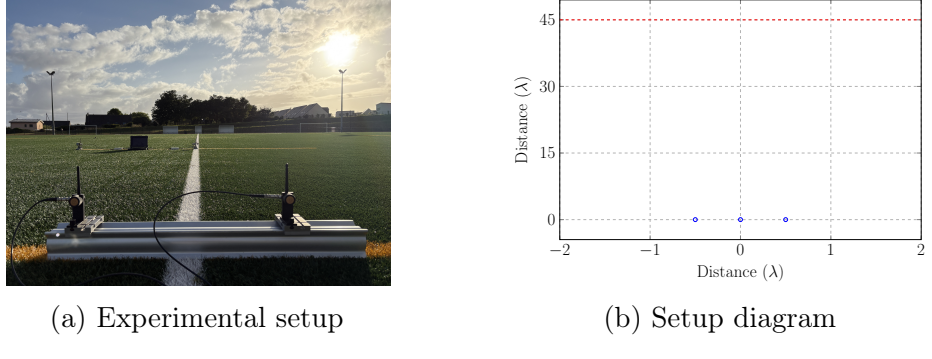


Figure 7.2: Diagram of the actual experimental setup.

the current arrangement, we observed that moving either the transmitter or receiver slightly near the source caused significant phase fluctuations, leading to a high variance in the DoA estimates. Even changes of a few centimeters at distances over 10 meters produced notable phase variations, making the measurements unstable for a single source. Additionally, differences in the heights of transmitting and receiving antennas also significantly affect the estimation results; varying the transmitter height between experiments could result in DoA estimation variances exceeding 20° . To address these issues, we used USRPs for transmission and reception, and carefully aligned the antenna heights prior to measurements. Fig. 7.2b illustrates the experimental layout, where the receiver antennas are marked as blue dots, and the transmitters are positioned near the red line, beyond the Fraunhofer distance from the receiving antennas. Moreover, environmental effects were found to be significant during the experiments. When performing DoA estimation indoors, the estimated directions often deviated considerably from the true values, even though the variance of the estimates was small. This discrepancy is likely caused by reflections from the surrounding environment.

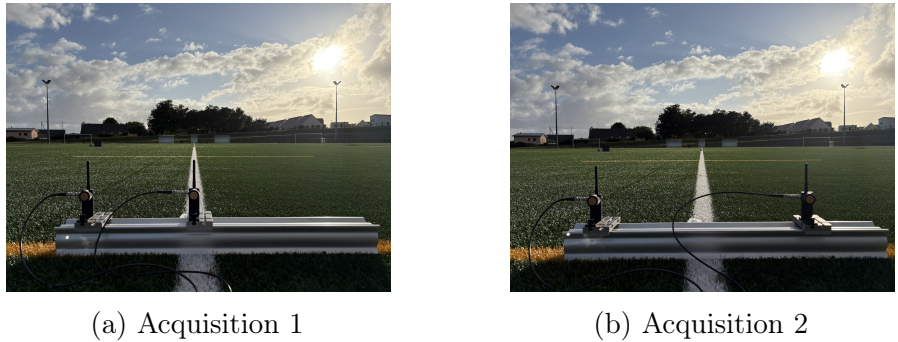


Figure 7.3: Virtual uniform linear array.

For the virtual ULA, we constructed a virtual array consisting of three antennas, as illustrated in Fig. 7.3, and used two transmitters. The transmitters emit QPSK signals, which are mutually uncorrelated.

7.3 Results

Fig. 7.4a, 7.4b shows the DoA estimation results using MUSIC with two antennas. The experiment was repeated ten times for each of tested angles. It was observed that the antennas are not truly omnidirectional and, at the distances described above, the received signal powers at the two antennas are not identical; these effects significantly impact the experimental outcomes. Detailed measurement data are reported in Appendix A. Nevertheless, from Fig. 7.4b it can be observed that, for the considered angles, both the variance and the RMSE of the estimated angle are on the order of 5° . According to the Cramér–Rao lower bound for DoA estimation, an ideal omnidirectional antenna yields the lowest RMSE near 0° , with the RMSE increasing as the incident angle departs from broadside. The deviations observed here from the theoretical trend are attributed to antenna directivity and environmental effects.

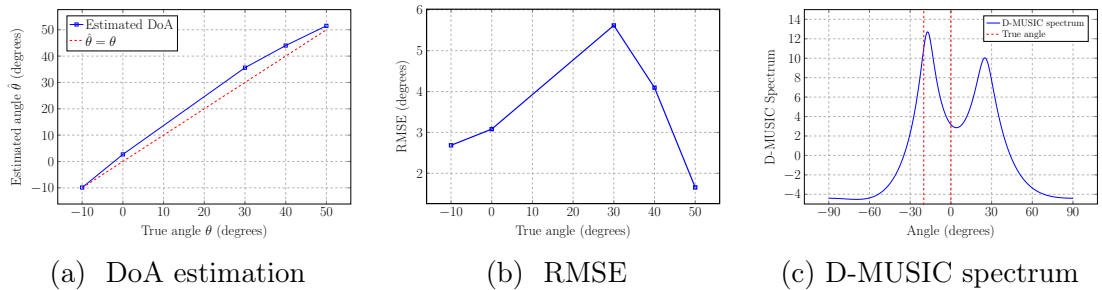


Figure 7.4: Experiment results.

Fig. 7.4c shows the D-MUSIC spectrum using a virtual 3-antenna array, where two peaks in the spectrum can be clearly observed. However, the estimation results are not accurate. Upon re-examining the received data, we found that when the two antennas are spaced by $\lambda/2$, and then the second antenna is moved while keeping the first antenna fixed to achieve a spacing of λ , the average power received by the first antenna differs by up to a factor of 10 between the two configurations. Examining the eigenvalues of the covariance matrix, we observed that the smallest eigenvalue is negative, which adversely affects the accuracy of the estimation.

Chapter 8

Conclusion

8.1 Summary of contributions

In this thesis, we proposed a method to enhance the DoF and to construct a virtual array of arbitrary geometry given $N_r \geq 2$ physical antennas. The effectiveness of this method was evaluated through simulations and compared with a physical array having the same DoF. Simulation results indicate that the proposed method can improve the estimation RMSE by increasing either the number of acquisitions or the number of snapshots. Moreover, this approach significantly enhances the resolution performance, even when compared to a physical array with the same DoF.

The proposed method increases the DoF without being limited by the number of physical antennas, unlike current array structures [9–19], which are inefficient when the number of physical antennas is small. Moreover, the virtual array constructed using our method can estimate the DoA of RF signals, a capability that is limited in [20–32] due to their requirement for high array speed. We performed optimization over the number of acquisitions for one-dimensional arrays and two-dimensional lattices, as well as DoF for one-dimensional arrays and the number of antennas required for two-dimensional arrays. The optimization results show that our method outperforms existing one-dimensional array structures, and the number of antennas needed to construct our difference co-array is optimal compared to current array designs.

We also evaluated the proposed method in the case of two sources and two antennas, where two distinct peaks were clearly observed in the spectrum. However, limitations in the antenna setup as well as the measurement environment adversely affected the estimation results.

8.2 Perspectives

As shown in Chapter 5, when a configuration solution is obtained using the CPLEX solver, a family of equivalent solutions can also be generated by translating all antennas within a finite number of acquisitions, by reflecting the entire antenna positions with respect to the array center, or by permuting the acquisitions. Each solution in this family generally corresponds to a certain number of antenna movements, and thus an additional optimization can be performed to select the best solution within the family in order to minimize the number of antenna relocations.

In addition, through the simulations presented in Chapter 6, I showed that when the coupling coefficient is on the order of 0.01, the system can be regarded as effectively uncoupled. As indicated in Chapter 2, an equivalent virtual array can then be constructed. Since the antennas in the virtual array are more sparsely spaced than those in the physical array, the impact of mutual coupling is reduced, which justifies investigating the coupling effects within the proposed virtual array construction method.

Moreover, although the estimation results in the case of two sources and two antennas were not fully accurate, two peaks were nevertheless identified. Possible factors affecting the estimation include electromagnetic interactions when antennas are placed in close proximity. Therefore, it is important to also examine their radiation patterns in this scenario to properly adjust the algorithm. In addition, the impact of reflections on DoA estimation can be mitigated by conducting experiments in an anechoic chamber.

References

- [1] H. Krim and M. Viberg. “Two decades of array signal processing research: the parametric approach”. In: *IEEE Signal Processing Magazine* 13.4 (1996), pp. 67–94. DOI: [10.1109/79.526899](https://doi.org/10.1109/79.526899).
- [2] M. Xiao et al. “Millimeter Wave Communications for Future Mobile Networks”. In: *IEEE Journal on Selected Areas in Communications* 35.9 (2017), pp. 1909–1935. DOI: [10.1109/JSAC.2017.2719924](https://doi.org/10.1109/JSAC.2017.2719924).
- [3] E. Björnson, L. Sanguinetti, H. Wymeersch, J. Hoydis, and T. L. Marzetta. “Massive MIMO is a reality—What is next?: Five promising research directions for antenna arrays”. In: *Digital Signal Processing* 94 (2019). Special Issue on Source Localization in Massive MIMO, pp. 3–20. ISSN: 1051-2004. DOI: <https://doi.org/10.1016/j.dsp.2019.06.007>. URL: <https://www.sciencedirect.com/science/article/pii/S1051200419300776>.
- [4] A. Fascista, A. Coluccia, H. Wymeersch, and G. Seco-Granados. “Millimeter-Wave Downlink Positioning With a Single-Antenna Receiver”. In: *IEEE Transactions on Wireless Communications* 18.9 (2019), pp. 4479–4490. DOI: [10.1109/TWC.2019.2925618](https://doi.org/10.1109/TWC.2019.2925618).
- [5] L. Godara. “Application of antenna arrays to mobile communications. II. Beam-forming and direction-of-arrival considerations”. In: *Proceedings of the IEEE* 85.8 (1997), pp. 1195–1245. DOI: [10.1109/5.622504](https://doi.org/10.1109/5.622504).
- [6] B. Van Veen and K. Buckley. “Beamforming: a versatile approach to spatial filtering”. In: *IEEE ASSP Magazine* 5.2 (1988), pp. 4–24. DOI: [10.1109/53.665](https://doi.org/10.1109/53.665).
- [7] R. Schmidt. “Multiple emitter location and signal parameter estimation”. In: *IEEE Transactions on Antennas and Propagation* 34.3 (1986), pp. 276–280. DOI: [10.1109/TAP.1986.1143830](https://doi.org/10.1109/TAP.1986.1143830).
- [8] X. Wu and W.-P. Zhu. “Single Far-Field or Near-Field Source Localization With Sparse or Uniform Cross Array”. In: *IEEE Transactions on Vehicular Technology* 69.8 (2020), pp. 9135–9139. DOI: [10.1109/TVT.2020.2998128](https://doi.org/10.1109/TVT.2020.2998128).

- [9] P. Pal and P. P. Vaidyanathan. “Nested Arrays: A Novel Approach to Array Processing With Enhanced Degrees of Freedom”. In: *IEEE Transactions on Signal Processing* 58.8 (2010), pp. 4167–4181. DOI: [10.1109/TSP.2010.2049264](https://doi.org/10.1109/TSP.2010.2049264).
- [10] W.-K. Ma, T.-H. Hsieh, and C.-Y. Chi. “DOA Estimation of Quasi-Stationary Signals With Less Sensors Than Sources and Unknown Spatial Noise Covariance: A Khatri–Rao Subspace Approach”. In: *IEEE Transactions on Signal Processing* 58.4 (2010), pp. 2168–2180. DOI: [10.1109/TSP.2009.2034935](https://doi.org/10.1109/TSP.2009.2034935).
- [11] P. Chevalier and A. Ferreol. “On the virtual array concept for the fourth-order direction finding problem”. In: *IEEE Transactions on Signal Processing* 47.9 (1999), pp. 2592–2595. DOI: [10.1109/78.782217](https://doi.org/10.1109/78.782217).
- [12] P. Chevalier, L. Albera, A. Ferreol, and P. Comon. “On the virtual array concept for higher order array processing”. In: *IEEE Transactions on Signal Processing* 53.4 (2005), pp. 1254–1271. DOI: [10.1109/TSP.2005.843703](https://doi.org/10.1109/TSP.2005.843703).
- [13] C. Zhou, Y. Gu, X. Fan, Z. Shi, G. Mao, and Y. D. Zhang. “Direction-of-Arrival Estimation for Coprime Array via Virtual Array Interpolation”. In: *IEEE Transactions on Signal Processing* 66.22 (2018), pp. 5956–5971. DOI: [10.1109/TSP.2018.2872012](https://doi.org/10.1109/TSP.2018.2872012).
- [14] X. Fan, C. Zhou, Y. Gu, and Z. Shi. “Toeplitz Matrix Reconstruction of Interpolated Coprime Virtual Array for DOA Estimation”. In: *2017 IEEE 85th Vehicular Technology Conference (VTC Spring)*. 2017, pp. 1–5. DOI: [10.1109/VTCSpring.2017.8108559](https://doi.org/10.1109/VTCSpring.2017.8108559).
- [15] C.-L. Liu and P. P. Vaidyanathan. “Hourglass Arrays and Other Novel 2-D Sparse Arrays With Reduced Mutual Coupling”. In: *IEEE Transactions on Signal Processing* 65.13 (2017), pp. 3369–3383. DOI: [10.1109/TSP.2017.2690390](https://doi.org/10.1109/TSP.2017.2690390).
- [16] S. Qin, Y. D. Zhang, and M. G. Amin. “Two-dimensional DOA estimation using parallel coprime subarrays”. In: *2016 IEEE Sensor Array and Multi-channel Signal Processing Workshop (SAM)*. 2016, pp. 1–4. DOI: [10.1109/SAM.2016.7569635](https://doi.org/10.1109/SAM.2016.7569635).
- [17] J. Shi, G. Hu, X. Zhang, and P. Gong. “Sum and difference coarrays based 2-D DOA estimation with co-prime parallel arrays”. In: *2017 9th International Conference on Wireless Communications and Signal Processing (WCSP)*. 2017, pp. 1–4. DOI: [10.1109/WCSP.2017.8171037](https://doi.org/10.1109/WCSP.2017.8171037).
- [18] Q. Wu, F. Sun, P. Lan, G. Ding, and X. Zhang. “Two-Dimensional Direction-of-Arrival Estimation for Co-Prime Planar Arrays: A Partial Spectral Search Approach”. In: *IEEE Sensors Journal* 16.14 (2016), pp. 5660–5670. DOI: [10.1109/JSEN.2016.2567422](https://doi.org/10.1109/JSEN.2016.2567422).

- [19] R. Rajamäki and V. Koivunen. “Sparse Active Rectangular Array With Few Closely Spaced Elements”. In: *IEEE Signal Processing Letters* 25.12 (2018), pp. 1820–1824. DOI: [10.1109/LSP.2018.2876066](https://doi.org/10.1109/LSP.2018.2876066).
- [20] Z. Zhang, Q. Shen, W. Liu, and W. Cui. “2-D DOA Estimation Based on Sparse Linear Arrays Exploiting Arbitrary Linear Motion”. In: *IEEE Transactions on Vehicular Technology* 73.9 (2024), pp. 13248–13262. DOI: [10.1109/TVT.2024.3392747](https://doi.org/10.1109/TVT.2024.3392747).
- [21] J. Ramirez and J. L. Krolik. “Synthetic aperture processing for passive coprime linear sensor arrays”. In: *Digital Signal Processing* 61 (2017), pp. 62–75. ISSN: 1051-2004. DOI: <https://doi.org/10.1016/j.dsp.2016.07.021>.
- [22] G. Qin, M. G. Amin, and Y. D. Zhang. “DOA Estimation Exploiting Sparse Array Motions”. In: *IEEE Transactions on Signal Processing* 67.11 (2019), pp. 3013–3027. DOI: [10.1109/TSP.2019.2911261](https://doi.org/10.1109/TSP.2019.2911261).
- [23] S. Li and X.-P. Zhang. “Dilated Arrays: A Family of Sparse Arrays With Increased Uniform Degrees of Freedom and Reduced Mutual Coupling on a Moving Platform”. In: *IEEE Transactions on Signal Processing* 69 (2021), pp. 3367–3382. DOI: [10.1109/TSP.2021.3083988](https://doi.org/10.1109/TSP.2021.3083988).
- [24] P. Ma, J. Li, J. Pan, X. Zhang, and R. Gil-Pita. “Enhanced DOA Estimation With Augmented CADiS by Exploiting Array Motion Strategies”. In: *IEEE Transactions on Vehicular Technology* 72.4 (2023), pp. 4713–4727. DOI: [10.1109/TVT.2022.3224908](https://doi.org/10.1109/TVT.2022.3224908).
- [25] Q. Shen, W. Liu, W. Cui, and S. Wu. “Underdetermined DOA Estimation Under the Compressive Sensing Framework: A Review”. In: *IEEE Access* 4 (2016), pp. 8865–8878. DOI: [10.1109/ACCESS.2016.2628869](https://doi.org/10.1109/ACCESS.2016.2628869).
- [26] C. Zhu, Y. Wang, and Q. Shen. “Two-Dimensional DOA Estimation Based on Two-Parallel Arrays Exploiting Nonuniform Array Motions”. In: *2022 IEEE 5th International Conference on Electronics Technology (ICET)*. 2022, pp. 723–727. DOI: [10.1109/ICET55676.2022.9824823](https://doi.org/10.1109/ICET55676.2022.9824823).
- [27] H. Wu, Q. Shen, W. Cui, and W. Liu. “DOA Estimation With Nonuniform Moving Sampling Scheme Based on a Moving Platform”. In: *IEEE Signal Processing Letters* 28 (2021), pp. 1714–1718. DOI: [10.1109/LSP.2021.3105035](https://doi.org/10.1109/LSP.2021.3105035).
- [28] J. Chu, Z. Zhang, Y. Huang, and Y. Guo. “A Novel Approach of 2-D DOA Estimation by Employing Coprime Linear Array Motion”. In: *IEEE Communications Letters* 26.1 (2022), pp. 69–73. DOI: [10.1109/LCOMM.2021.3123976](https://doi.org/10.1109/LCOMM.2021.3123976).
- [29] X. Li, W. Wang, X. Wang, and S. Ren. “Synthetic sparse planar array design for two-dimensional DOA estimation”. In: *Digital Signal Processing* 120 (2022), p. 103268. ISSN: 1051-2004. DOI: <https://doi.org/10.1016/j.dsp.2021.103268>.

- [30] G. Qin, Y. D. Zhang, and M. G. Amin. “DOA Estimation Exploiting Moving Dilated Nested Arrays”. In: *IEEE Signal Processing Letters* 26.3 (2019), pp. 490–494. DOI: [10.1109/LSP.2019.2894467](https://doi.org/10.1109/LSP.2019.2894467).
- [31] G. Wang, Z. Fei, and S. Ren. “2D DOA Estimation Exploiting Vertical Synthetic Planar Arrays”. In: *IEEE Access* 9 (2021), pp. 3497–3507. DOI: [10.1109/ACCESS.2020.3047686](https://doi.org/10.1109/ACCESS.2020.3047686).
- [32] Y. Zhou, Y. Li, and C. Wen. “The Multi-Level Dilated Nested Array for Direction of Arrival Estimation”. In: *IEEE Access* 8 (2020), pp. 43134–43144. DOI: [10.1109/ACCESS.2020.2977105](https://doi.org/10.1109/ACCESS.2020.2977105).
- [33] J. Xin, G. Liao, Z. Yang, and H. Shen. “Ambiguity Resolution for Passive 2-D Source Localization with a Uniform Circular Array”. In: *Sensors (Basel, Switzerland)* 18 (2018). URL: <https://api.semanticscholar.org/CorpusID:52005268>.
- [34] C.-L. Liu and P. P. Vaidyanathan. “Two-dimensional sparse arrays with hole-free coarray and reduced mutual coupling”. In: *2016 50th Asilomar Conference on Signals, Systems and Computers*. 2016, pp. 1508–1512. DOI: [10.1109/ACSSC.2016.7869629](https://doi.org/10.1109/ACSSC.2016.7869629).
- [35] M. Ebrahimi and S. Gazor. “Two-Dimensional Minimum Sensor Array: A New Perspective to Array Design”. In: *IEEE Sensors Journal* 23.13 (2023), pp. 14685–14690. DOI: [10.1109/JSEN.2023.3273401](https://doi.org/10.1109/JSEN.2023.3273401).
- [36] X. Liu and N. Sidiropoulos. “Almost sure identifiability of constant modulus multidimensional harmonic retrieval”. In: *IEEE Transactions on Signal Processing* 50.9 (2002), pp. 2366–2368. DOI: [10.1109/TSP.2002.801933](https://doi.org/10.1109/TSP.2002.801933).
- [37] T. Jiang, N. Sidiropoulos, and J. ten Berge. “Almost-sure identifiability of multidimensional harmonic retrieval”. In: *IEEE Transactions on Signal Processing* 49.9 (2001), pp. 1849–1859. DOI: [10.1109/78.942615](https://doi.org/10.1109/78.942615).

Appendix A

Experimental results

This chapter presents the experimental data for DoA estimation. For each angle, the estimation was performed 10 times.

Table A.1: DoA estimation results using MUSIC for a single source.

True angle	Estimated angle									
-10	-12.3922	-11.3908	-12.1419	-14.1446	-10.8901	-9.8887	-7.6356	-4.8818	-7.8860	-7.6356
0	2.8790	3.6300	5.1321	3.8804	2.6287	4.1307	2.6287	0.6259	0.6259	0.6259
30	35.9249	35.4242	36.1752	36.1752	36.1752	35.4242	34.9235	35.1739	35.1739	35.4242
40	43.9360	43.6857	43.1850	44.1864	43.4353	42.6843	43.6857	45.4381	44.9374	44.9374
50	51.6968	50.9458	51.4465	50.9458	51.1961	50.9458	50.4451	52.4478	52.1975	52.6982